Tracing the HIMU component within Pan-African lithosphere beneath northeast Africa: Evidence from Late Cretaceous Natash alkaline volcanics, Egypt

M.A. Abu El-Rus, G. Chazot, R. Vannucci, Jean-Louis Paquette

Tracing the HIMU component within Pan-African lithosphere beneath northeast Africa: evidence from Late Cretaceous Natash alkaline volcanics, Egypt

Abu El-Rus, M.A. [(1)], Chazot, G.[(2)] , Vannucci, R.[(3)], Paquette J.-L.[(4)]

(1) Geology Department, Faculty of Science, Assiut University, 71516, Egypt

(2) Université de Brest (UBO), UMR 6538, Géosciences Océan, Institut Universitaire Européen de la Mer (IUEM), place Copernic, 29280 Plouzané, France.

(3) Dipartimento di Scienze della Terra e dell'Ambiente, Università di Pavia, Via Ferrata 1, 27100 Pavia, Italy

(4) Laboratoire Magmas et Volcans, Université Blaise Pascal – OPGC, 63038 Clermont-Ferrand, France

Abstract

A large late Cretaceous (~ 90 Ma) volcanic field (the Natash volcanic province) crops out in southeast Egypt, the northwestern boundary of the Arabian-Nubian shield. The lavas are mainly of alkaline affinity and exhibit a continuous compositional range from alkali olivine basalt (AOB) to trachyte and rhyolite. All lavas in the province record various extents of fractional crystallization of olivine, clinopyroxene, plagioclase and spinel. The basaltic lavas show variations in Sr-Nd-Pb-Hf isotopic ratios [$(^{87}Sr/^{86}Sr)_i$ = 0.7030 - 0.70286; $(^{143}Nd/^{144}Nd)_i$ = 0.512653-0.512761; $(^{206}Pb/^{204}Pb)_i$ = 19.28--19.944; $(^{177}Hf\text{-}^{176}Hf)_i$ = 0.28274-0.28285], that correlate markedly with the major and incompatible trace element ratios and abundances. Assimilation of crustal material cannot explain these correlations, and we invoke instead melting of a multicomponent mantle source. We infer the existence of High-μ (HIMU), Enriched Type I (EM I) and Depleted (DM) mantle domains in the melting source, with a predominant contribution from the HIMU-type. We

suggests further that the basaltic lavas originate from low degrees of partial melting (F < 5%) at moderate potential temperatures (T_P) 1391 -1425 ^oC and pressures of 2.0-2.6 GPa. The melting pressure estimations imply that melting entirely occurred within lithospheric mantle, most likely in the presence of residual amphibole as negative K-anomalies in the primitive mantle-normalized patterns of the fractionation-corrected melts. The presence of amphibole within the lithosphere is a strong evidence that the lithospheric mantle underwent metasomatic enrichment prior to melting in Late Cretaceous. This metasomatic event is inferred to affect Pb isotopic compositions of the Natash volcanics by adding Th and U to the source domain. Time-integrated calculations to remove the decoupling between ^{206}Pb and ^{207}Pb isotopes that most probably resulted from the metasomatic event indicate a tentative link between the metasomatism occurring in the Pan-African lithospheric mantle and the formation of juvenile crust during the Pan-African Orogeny. A two stages evolution model is therefore proposed for volcanism in the Natash area: fluxing of the lithosphere by hydrous fluids during Pan-African Orogeny formed a hybrid lithospheric mantle that in Late Cretaceous underwent thermal erosion and melting in response to upwelling asthenosphere, possibly at the onset of the extensional fracturing preceded the doming of the Afro-Arabian Shield.

Keywords: *Lithospheric mantle, metasomatism, partial melting, potential temperature, fractional crystallization, High-μ mantle (HIMU), Depleted Mantle (DM), Enriched Mantle (EM-I)*

1. Introduction

Two alternative hypotheses (passive and active tectonics) have been considered to explain the common sequence of thinning, rifting and eventual break-up of the continental lithosphere: passive rifting assumes that extension is ruled by pure or simple shear, while active rifting assumes that the extension process is dominated by thermal erosion at the base the lithospheric mantle as consequence of arrival of thermal anomalies such as mantle plumes (e.g., Fitton, 1983; Turcotte, 1989). In the passive rifting model the subcontinental lithosphere is physically replaced by asthenospheric material and thus it is not involved (or just at a very limited extent) in the generation of basaltic magmas; in contrast, in the active rifting models basaltic magmas may form from the lithospheric mantle alone or from the interaction (mixing) between sub-lithospheric mantle (ambient asthenosphere or upwelling plumes) and the lithospheric mantle materials (e.g. both reservoirs contribute to magma genesis; e.g., Leeman and Fitton, 1989; Altherr et al., 1990; Huismans et al., 2001; Thybo and Artemieva, 2013; Rooney, 2017). Whatever the mechanism, continental rifts are initially characterized by relatively broad zones of 'mechanical' extension in which faulting and stretching of the lithosphere accommodates the strain (Rooney et al., 2011). This extension process is likely accommodated by triggering melting within the lithospheric plate prior to rupture, without marked crust thinning (e.g., Ebinger et al., 1993; Mackenzie et al., 2005; White et al., 2008; Thybo and Nielsen, 2009, Rooney et al., 2011). However, triggering melting at the onset of rifting is enigmatic as only minor decompression is expected for limited degrees of extension. For this reason, other mechanisms for inducing melting in subcontinental mantle have been proposed, such as a deep-seated thermal anomaly, the presence of volatiles, and/or a pre-existing chemical heterogeneity in either the asthenosphere or in the continental

lithosphere (e.g,. White et al., 1987; McKenzie and Bickle, 1988; Sleep 1996; King and Ritsema, 2000; Class and Le Roex, 2006; Rooney, 2017).

The Afro-Arabian Dome encompasses portions of the East African Rift System (EARS) that record many different stages of rift evolution from rift initiation to break-up and embryonic oceanic spreading as manifest in the Afar depression, at the Red Sea, Gulf of Aden junction, the Turkana depression and the Main Ethiopian Rift as well as individual off-rift volcanic fields (e.g., Almond, 1986a, b; Ebinger, 2005; Corti, 2009) (Fig, 1a). The Afro-Arabian Dome is therefore an ideal place to analyse the dynamics by which continental lithosphere progressively breaks up into oceanic spreading centres. The transitional (Ethiopian and Yemen trap series) to tholeiitic (Red Sea) volcanism is associated with crustal extension in Arabia and NE Africa that initiated in the Late Cretaceous along northwest trending faults and continued into the Oligo-Miocene with the subsequent development of the Red Sea basin. In contrast, the uplift producing the Afro-Arabian Dome began in the Miocene and is associated with prevailing alkaline volcanism along N-NE trends in Africa and N-S trends in Arabia (e.g., Almond, 1986 a,b; Bosworth et al., 2005; Avni et al, 2012).

Whereas the Sr-Nd-Pb isotope compositions of basalts from the western Arabian plate the Red Sea and the Gulf of Aden, and those occurring in the Afar, Turkana depressions and Main Ethiopian Rift are now well constrained (e.g., Altherr et al., 1990; Barrat et al., 1990, 1993; Schilling et al., 1992; Volker et al., 1993, 1997, Shaw et al., 2007; Krienitz et al., 2009; Rooney et al.,2012), this is not the case for sporadic basalt eruptions in northeast Africa whose isotopic signatures are commonly unknown. In this paper we aimed at updating our knowledge on the Late Cretaceous Natash volcanics

(85.6 ± 3 Ma. K/Ar age for an alkali basalt flow, El-Shazly and Krs, 1973), that form the largest lava province erupted at the western margin of the Afro-Arabian Dome in southern Egypt (Fig. 1b) and are, therefore, of great importance in understanding the ongoing differentiation and dynamics within the Earth during the early stages of the continental rifts. Detailed chemical, but not isotopic, studies of Natash volcanics highlighted the role of fractional crystallization in the differentiation of primary magmas (e.g., Hashad and El-Reedy, 1979; Ressetar et al., 1981; Hashad et al. 1982; Crawford et al., 1984; Hubbard et al., 1987; Hashad, 1994; Mohamed et al., 2001), which most probably took place in multiple short-lived chambers beneath the Natash field rather than in an individual long-lived chamber (Mohamed, 2001). Crustal contamination was also involved in the formation of some volcanics at later stages of the fractionation process (Hashad et al. 1982). In the present paper, we present new bulk-rock and mineral analyses, as well as radiogenic isotope data, for a selection of most basic flows from the Natash volcanic field to unravel the role of mantle source heterogeneity, the relative contributions of asthenospheric and lithospheric mantle, and the depths and degrees of partial melting. The whole data set is discussed to make inferences on the deep-seated processes associated with initiation of rifting and doming in the Afro-Arabian plate.

2. Geological Setting

The Natash volcanics cover an area of ~ 560 km^2 (Crawford et al., 1984) located at the margin of the juvenile Arabian-Nubian shield in the south-eastern Egypt (Fig. 1b). The volcanic field is made up by a number of sub-horizontal lava flows, up to 20 m thick each, commonly intercalated with the Cretaceous Nubian sandstone that also bound the

western, northern and partly southern boundary of the field (Fig.2). On the east and partially along the southern border, the Natash volcanic field is juxtaposed against basement rocks directly by high angle normal faults (Fig. 1b)

Three distinct volcanic flow units are recognized (Fig. 1b), which are separated by two sequences of volcanoclastic sediments or by basal polymictic conglomerate beds indicating temporal breaks in the eruptive sequence (Carwford et al., 1984, Madani, 2000; Mohamed, 2001). Crawford et al. (1984) defined a third volcanoclastic unit locally, capping the upper flow unit from the east that may be covered by trachyte flows. Erosion has removed the upper flow unit and the upper volcanoclastic sequence from most localities in the central and eastern parts of the Natash province. The volcanoclastic tuffs intercalated between lava flows are frequently fining upward, usually encompassing sparse wood fragments and leaf imprints of Cenomanian age (Crawford et al., 1984), whereas each of the lava flow units shows a gradual change upwards from grey-green, porphyritic flows to vesicular, aphyric black flows. Several trachyte plugs found, primarily in the eastern area, forming horse shoe-ring and dome-like structures up to 100 meters height and hundreds of meters in diameter. Sometimes, the trachyte domes are surrounded by high-density, consolidated pyroclastic deposits. They are mostly distributed along NE-SW linear trends that seem to be structurally controlled by older faults of the Nubian Shield (Hashad, 1994). The plugs are made of massive, aphyric and poorly vesiculated rocks, commonly greenish to brownish in colour. Volcanic bombs and tuffs were observed in one trachyte plug volcanic bombs.

Rounded to subangular peridotite xenoliths, up to 15 cm in diameter have been found in the basalts of the lower lava flows unit at ~ 24^{o} 25′ 56.4″ N and 33^{o} 59′ 34.4″ E

(Madani, 2000; Abu El-Rus et al., 2016). The xenoliths belong to the Cr-diopside group and are largely altered to serpentine, carbonates, chlorite, secondary amphibole and clay minerals. Notwithstanding, large parts of diopside grains are frequently well preserved in all xenoliths, allowing investigation of the partial melting event and successive chromatographic enrichment by carbonatite-like melts (Abu El-Rus et al., 2016). The steep P-T gradient estimated by clinopyroxene geothermobarometry and the close geochemical similarity between carbonatite melts equilibrated with the Natash mantle xenoliths and the plume-derived Cretaceous carbonatite complexes from east Africa (Bizimis et al., 2003) are consistent with the presence of a mantle plume at the base of the lithosphere after its accretion to the Arabian-Nubian Shield in Late Precambrian (Abu El-Rus et al., 2016).

3. Analytical techniques

Bulk-rock samples were analyzed for major, minor and selected trace element abundances on the Horiba-Jobin-Yvon Ultima 2 ICP-AES at the European Institute for Marine studies, Pôle de Spectrométrie Océan, Brest, France (PSO-IUEM). The detailed description of the analytical procedure is given by Cotten et al. (1995). Elements were determined from an H_3BO_3 solution, boron being used as internal standard for ICP-AES analysis. For major elements, relative standard deviation is 1% for SiO_2 and 2% for the other major elements, except for low values (<0.50 wt %), for which the absolute standard deviation is ±0.01 wt%. All major oxides used in diagrams and reported in the present text are normalized on an anhydrous basis and total iron recast as FeO.

Trace element concentrations were measured with a Thermo Element2 HR-ICP-MS in Brest (France), after ~~a~~ repeated HF-$HClO_4$ digestion and HNO_3 dilutions (see Li and Lee 2006 for details). The repeated analysis of the international standards BIR1 and BCR2 demonstrated an external reproducibility better than 5–10 % depending on the element and concentration (Table A1). The major and trace elements compositions of the selected Natash basic flows are shown in Table 1.

Sr and Nd isotope ratios were measured in static mode using a solid source Thermo Fisher® Triton TI-MS (Thermal Ionization-Mass Spectrometer) at PSO-IUEM. All measured ratios were corrected for fractionation using $^{88}Sr/^{86}Sr = 8.3752$ and $^{146}Nd/^{144}Nd = 0.7219$. Pb and Hf isotopic ratios were measured using a Thermo Fisher® Neptune MC-ICP-MS (Multi Collector-Inductively Coupled Plasma- Mass Spectrometer) at PSO-IUEM. The Hf mass bias was corrected using an exponential law and assuming a $^{179}Hf/^{177}Hf$ ratio of 0.7325. Pb isotopic ratios were measured using the thallium addition technique in order to correct for mass bias (White et al., 2000). The NIST981 standard was run every two to three samples to correct all Pb isotopic ratios by standard bracketing with the value recommended by Galer and Abouchami (1998). The isotopic data are presented in Table 2.

Major element composition of phenocrysts in selected samples (Tables A2-A5) was determined by a CAMECA CAMEBAX SX100 electron microprobe at the Laboratoire Géosciences Océan (University of Brest) using a 15 kV and 10nA beam focused to a spot of ~2 μm in diameter. The peaks were counted for 10s and backgrounds for 5s. Light elements were counted first to preclude loss by volatilization. Oxides, natural mineral and synthetic standards have been used. Matrix corrections were performed by the PAP-

procedure in the CAMECA software. Analytical precision (± 2 sigma error) evaluated by repeated analyses of individual grains is better than ±1% for elements with concentrations ≥20 wt.% oxide, better than ±2% for elements in the range 10–20 wt% oxide, better than 5% for elements in the range 2-10 wt, % oxide, and better than 10% for elements in the range 0.5-2 wt, % oxide.

4. Results

4.1 Petrography and mineral chemistry

Natash mafic lavas contain variable amounts of phenocrysts and microphenocrysts of olivine, clinopyroxene and plagioclase. Some lavas—display glomerocrysts of clinopyroxene, olivine and plagioclase. Apatite microphenocrysts are observed in sample NAT-14, whereas sparse quartz xenocrysts rimmed by thin reaction rinds and spinel phenocrysts are observed in sample NAT-13. The groundmass is usually fine grained, with a pilotaxitic texture dominated by plagioclase laths prismatic clinopyroxene and granular Fe-Ti oxides together with subordinate amounts of intergranular olivine. Fine shreds of biotite are present only in the groundmass of samples–NAT-08. Rare empty vesicles are also visible in some samples.

Olivine typically occurs as rounded phenocrysts of variable size, up to 6 mm across and as fine blebs embedded in the groundmass. At margins and along cracks olivine is partially to entirely replace by yellowish to reddish-brown iddingsite. In general, olivine shows a wide compositional range, both across the sample suite and at the thin-section scale. Forsterite contents are Fo 86 -70 for phenocryst cores and Fo75-48 for the olivine in the groundmass. Most of the olivine phenocrysts show normal zoning, generally with a

14% decrease in Fo content from core to rim (Table A2). Some of the cores contain small spinel inclusions (sample NAT-13, Table A5). In general, the phenocryst cores do not approach equilibrium with the bulk-rock compositions, using $^{ol\text{-}Liq}D_{Fe\text{-}Mg}$ between 0.26 and 0.36 (Roeder & Emslie, 1970); the bulk chemistry is Mg-poor to be in equilibrium with olivine phenocrysts, suggesting significant accumulation of ferromagnesian minerals during ascending.

Clinopyroxene occurs in all samples either as phenocrysts of variable size, up to 10 mm long and as microlite in the groundmass. The phenocrysts are typically anhedral, exhibit disequilibrium outlines with the host magma and frequently form glomerocrysts with olivine and plagioclase. The core compositions do not match experimentally determined $^{cpx\text{-}melt}D_{Fe\text{–}Mg}$ values (0.23–0.30; Bryan et al.1981; Tormey et al. 1987; Putirka et al. 2003). We note that the clinopyroxene phenocrysts lack evidence of deformation (e.g. kink-bands) that would be expected in xenocrysts of lithospheric mantle origin (e.g., Neumann et al., 2015), and suggest that they crystallized at depth from more primitive magma batches and were subsequently incorporated into a more evolved magma. The majority of clinopyroxenes is augite, but some are dioposide, following the classification of Morimoto et al. (1988) (Fig. A1). The phenocrysts exhibit wide normal zoning with decreasing En and increasing Wo and Fs contents from core to rim. The groundmass clinopyroxenes commonly have higher Wo and Ti and lower En and Al contents relative to the core of phenocrysts. The single-pyroxene geobarometer of Nimis (1995) and Nimis and Ulmer (1998) indicate a wide range of values for equilibrium crystallization P when applied to clinopyroxene cores (~1.4-7.1 kbar); negative pressure estimates are obtained for the phenocryst rims and groundmass microlites, implying that their

crystallization occurred at shallow level, i.e. below than the uncertainties of these geobarometers (~ 2 kbar Nimis, 1995&; Nimis and Ulmer, 1998; Table A3).

Plagioclase is the dominant phenocryst in Natash mafic lavas, although it is not found in samples NAT-3, NAT-8 and NAT-13. The phenocrysts are sub-idiomorphic to idiomorphic and commonly have linear boundaries in equilibrium with the host lava. They are typically labradorite (An $_{4\text{-}58}$, core), but the most fractionated sample NAT-14 andesine (An_{34}, core). The phenocrysts frequently exhibit normal zoning with An contents decreasing by several percent at the rim. Plagioclase in the groundmass form microlites interstitial with augite, olivine and titanomagnetite grains. Compared with the phenocryst cores in the same sample, the microlites extend their composition to lower An contents (An $_{62\text{-}24}$).

Fe-Ti oxides are ubiquitous in the groundmass of all samples and sometimes form large phenocrysts up to 5 mm across. They display a wide compositional rangeTiO_2 (21.4-39.1 wt. %) and FeO_T (54.0-69.3 wt. %). In the most primitive sample NAT-13 oxides occurring as phenocrysts are Al-rich (Al_2O_3 =29.2 wt. %) and Ti-poor (TiO_2 =13.8 wt. %). One inclusion in olivine in this sample is a spinel ($MgAl_2O_4$)-ercinite ($Fe^{2+}Al_2O_4$) solid solution.

4.2 Major and trace elements

All the analyzed samples have loss-on-ignition (LOI) values < 2.25 wt% and appear to be fresh with little or no alteration under microscope. Likewise, no correlation exists between LOI and the amounts of CaO and incompatible mobile elements such as K, Na, Rb and U, suggesting that the effects of alteration are negligible. The Natash

mafic flows have 44-47.4 wt. % SiO_2 and total alkalis from ~3.6 to 6.4 wt. % (Table 1), categorizing them as olivine alkali basalts, basanites and trachybasalts (Fig. 2). Their bulk compositions are nepheline normative, but samples NAT-5 and NAT-11 are hypersthene-normative. Mg-number ranges from 0.45 to 0.61, but samples NAT-12 and NAT-14 have lower Mg-numbers as low as (0.39 and 0.33, respectively). The Mg-number is strongly correlated with major, transition and mildly incompatible elements and fairly well with large ion lithophile (LIL) elements (e.g. Ba, Rb, Cs, Sr; Fig.4 3).

The Natash lavas display steep primitive mantle-normalized REE patterns [$(La/Lu)_N$ =13 -18)], commonly with marked fractionation in HREE [$(Dy/Lu)_N$ = 2.1-2.5; Fig. 4]; suggesting equilibration with residual garnet. No Eu anomaly is found in any of the samples. Primitive-mantle normalized multi-element plots (Fig. 5) display the overall shape of OIB patterns, with upward-concavity in the highly incompatible peaks at Ta and Nb, and troughs at K and Pb. Such patterns are typically observed in HIMU-type OIB basaltic lavas (Kogarko et al., 1984; Newsom et al., 1986; Weaver et al., 1987; Chaffey et al., 1989; Thirlwall, 1997; Willbold and Stracke, 2006)

4.3 Radiogenic isotopes

When considering 90 Ma-corrected initial ratios (Table 2), the Natash lavas display more depleted $^{87}Sr/^{86}Sr$ (Sr_i= 0.70286 - 0.70305); $^{143}Nd/^{144}Nd$ (Nd_i= 0.512653 - 0.512761) and $^{176}Hf/^{177}Hf$ (Hf_i = 0.28274 -0.2829), and more radiogenic $^{206}Pb/^{204}Pb_i$ (19.28-19.94), $^{207}Pb/^{204}Pb_i$ (15.68-15.74) and $^{208}Pb/^{204}Pb_i$ (39.05- 39.47) compared to the local MORB (Red Sea and Gulf of Aden ridges), Plio-Pleistocene Afar lavas and other Arabian and North African intraplate volcanics (Figs. 5). The Natash lavas define a tight

array plot marginally to the isotopic field of the Arabian lithospheric mantle (5a and b). This trend contrasts with that of intraplate basalts from across the Arabian Plate (Bertrand et al. 2003, Endress et al., 2010), which define an elongate field that broadly overlaps the mantle array and extends towards MORB-like values. In terms of $^{208}Pb/^{204}Pb$ and $^{206}Pb/^{204}Pb$ values, the Natash lavas have initial ratios similar to those of the most radiogenic Red Sea MORB from axial trough and Ramad seamount (Barrat et al., 1990, Schilling et al., 1992; Volker et al., 1993) and overlap the composition of the Arabian lithospheric mantle. In contrast, they display higher $^{207}Pb/^{204}Pb$ values relative to the Arabian lithospheric mantle and plot considerably above the North Hemisphere Reference Line (NHRL; Fig. 5C). Overall, the isotopic ratios exhibit broad correlations with the abundance of several elements (e.g. MgO and SiO_2) as well as with the ratios of several incompatible element ratios (e.g. Ce/Pb and U/Nb; Fig. A2), suggesting melting of ~~an~~ a heterogeneous source or a role of crustal contamination processes.

5. Discussion

5.1 The role of fractional crystallization

The Natash basalts show variable amounts of olivine, clinopyroxene and plagioclase phenocrysts. Despite their limited variation in silica contents, they exhibit a wide range of relatively low Mg# values and Ni and Cr contents (Table 1). These features imply that none of the lavas can be considered as primary melt and that crystal fractionation played a significant role during magma ascent. Therefore, the chemical effects of fractional crystallisation should be corrected before exploring constraints on the mantle source and melting conditions. According to both textural and chemical evidence,

namely the presence of corroded olivine, clinopyroxene and spinel phenocrysts and the very low Ni and Cr contents, the liquid-line of descent of the Natash lavas should be corrected for olivine, clinopyroxene and Cr-spinel crystallisation. In contrast, evidence for plagioclase fractionation is lacking due to the absence of Eu anomalies in the sample suite (Fig.~~5~~ 4). Moreover, the presence of euhedral plagioclase phenocrysts indicates their late crystallization in equilibrium with the host magma at shallow level, making unnecessary of the plagioclase-correction. Based on the textural features of olivine and clinopyroxene described above and the wide range of equilibrium pressures estimated by single clinopyroxene geobarometer, we deduce that the Natash magmas ponded ~~up~~ and fractionated at different depths within the crust during evolution prior to eruption.

To remove the effect of fractional crystallization on the geochemical signatures of the Natash primary melts we used the Petrolog model (version 3.1.1.3; http://petrolog.web.ru/latest.html) (Danyushevsky & Plechov, 2011), based on the concept of pseudo-liquidus temperatures (Nathan and Van Kirk, 1978; Nielsen and Dungan, 1983; Ariskin et al., 1986). The method relies on the ability of the mineral-melt equilibria models to calculate liquidus temperature not only for the range of melt compositions where the minerals are stable, but also in the metastable regions of melt compositions for each phase (Danyushevsky and Plechov, 2011). Amounts of the relevant liquidus phases (olivine, clinopyroxene and cr-spinel) are added back to the measured compositions to attain the primary melt composition that meets requirements to be in equilibrium with mantle olivine (i.e. Mg# 0.68-0.72, 300-500 ppm Ni, > 750 ppm Cr; e.g., O'Hara, 1968; Albarède, 1992, Frey et al., 1978; Herzberg and O'Hara, 2002; Green and Falloon, 2005; Niu and O'Hara, 2007). The calculations were performed

assuming polybaric crystallization with an initial pressure as low as 0.5 kbar continuously increased up to 7.1 kbar as suggested by the core to rim compositional variation of clinopyroxene phenocrysts**.** The range of fO_2 values was set assuming that Fe_2O_3/TiO_2 varies from 0.5 to1.0, representing respectively the lower (reducing) and upper (oxidizing) limits of fO_2 , expected for crystallization of most of the continental plate basalts (Rooney et al., 2012, Abu El-Rus and Rooney, 2016). Assumptions and parameters used in running Petrolog 3.1.1.3 program are presented in Appendix D. The amount of mineral phase added to each calculation step is 0.01%. Though the Petrolog software minimizes the potential impact of fractional crystallization, some bias in the calculation of the hypothetical primary magma composition may result either from the uncertainty in choosing mineral-melt partition values and/or from the proposed stages at which the liquidus phases join or leave the liquid line of descent. However, the systematic variation among elements (Fig. 6a), the tightness of the REE and incompatible trace elements patterns of the calculated melt fractions (Fig. 4) and the preservation of several trace element ratios (e.g.Ta/Nb; La/Nb, Fig. b,c) during the fractionation path give us confidence that the modelling calculations are reasonable. The calculations indicate olivine as liquidus phase only at melt Mg# > 0.7 and the dominant role of clinopyroxene fractionation in the modification of primary magma composition of Natash lavas (Appendix D; Table A7). These numerical estimates are largely consistent with the predominance of clinopyroxene phenocrysts over other mineral phases in all Natash basalts. The fractional crystallization modelling also indicates that the majority of Natash lavas initially were hypersthene normative (Appendix D) and acquired most of their alkalinity during the fractionation process. Finally, Figure 6a shows that several

fractionation-corrected melts in the range of 0.68-0.72 Mg# do not meet the requirements expected for primary melts (i.e., Ni >320 ppm; Ni/MgO >25; Cr >750 ppm; e.g. Sato, 1977; Hart and Davis, 1978, Herzberg and O'Hara, 2002; Green and Falloon, 2005). Therefore, these melt compositions are not considered appropriate to discuss source composition and melting parameters.

5.2 Crustal contamination versus source heterogeneity

All the investigated samples contain variable amounts of zoned phenocrysts that are also embayed and corroded by groundmass. These textural features clearly ~~testify~~ indicate that the Natash magmas ponded at a depth within the crust after their segregation from the mantle source and during their ascent to the surface. As a result, the ascending magma may have been affected by assimilation of crustally-derived materials, a process that can impart profound modifications to the primary melt composition. Studies on the composition and age of crustal xenoliths within Natash volcanics are lacking, yet a Late Proterozoic age is reported for the basement rocks in the surrounding area (e.g., El-Gaby et al. 1988; Kröner et al. 1992; Khudier et al. 2006; 2008). This suggests that a Late Proterozoic crust is likely present beneath the Natash volcanic province. Isotope evidence (Fig. A3a) indicates that a Late Proterozoic lower crust (granulite facies) such as that occurring in Saudi Arabia and Zabargad Island is a more plausible contaminant relative to other crust-derived rocks from the Afro-Arabian Shield such as mafic granulites from Tanzania, Sudan and Yemen. On this basis, we performed bulk mixing and assimilation-fractional crystallization (AFC) calculations using the average composition of the Late Proterozoic mafic granulites from Saudi Arabia and Zabargad gneiss complex (Table-3)

and samples NAT-13 and NAT-14, which represent the most and least primitive composition among the data set (Table 2). The calculations reveal that none of the investigated samples plots along AFC or bulk mixing trajectories (Fig. 7), leading us to conclude that the range of isotope ratios shown by the Natash lavas cannot be ascribed to the assimilation of crustally-derived material. Rather, it is most likely a signature inherited from a heterogeneous mantle source. This conclusion is further supported by the plot of Natash lavas within the range observed globally for primitive mantle-derived basalts on Ta/Yb and Th/ Yb diagram (Fig. A4). Other chemical features that can be hardly reconciled with crust assimilation processes are the presence of negative Pb and K anomalies in the primitive mantle-normalized patterns (Fig. 4), the positive correlation between SiO_2 and $^{143}Nd/^{144}Nd$ (Fig. A2a), and the negative correlation between Ce/Pb and $^{87}Sr/^{86}Sr$, (i.e. two major indexes of crust contamination (Fig. A2b). Moreover, the occurrence of mantle peridotite xenoliths within the lavas provides additional evidence on the rapid ascent of the Natash magmas through open conduits without/ or with minor) interaction with the continental crust.

In summary, although we cannot rule out completely incorporation of crust material during the ascent of various magma batches, the above considerations strongly favour the view that the geochemical variations shown by the Natash lavas mostly reflect a heterogeneity within the mantle source region rather than crustal contamination effects.

5.3 Constraints on the melting source

a. Amphibole-bearing source

The significant K depletion relative to the neighbour elements observed in the PM-

normalized trace element patterns of the fractionation-corrected melts is striking evidence for either fractionation of a K-rich mineral (e.g. amphibole or phlogopite) from primary melts or the presence of these K-bearing phases in the melting mantle source. Amphibole and phlogopite phenocrysts are never observed; moreover, their crystallisation requires high water contents and high fO_2 values that would lead to the expansion of the olivine primary phase field over other minerals (e.g., Sisson and Grove, 1993), a feature at odd with the predominant fractionation of clinopyroxene over olivine evidenced by Petrolog calculations for the lavas from the Natash volcanic province. We therefore conclude that the presence of a residual hydrous K-rich phase in the melting source is the most plausible explanation for the observed negative-K anomaly in the Natash mafic lavas.

To constrain whether the lava source is an amphibole- or a phlogopite-bearing mantle sector, we explore the interrelationships between Nb, Rb and Ba (e.g., Späth et al.1996; 2001; Abu el-Rus and Rooney, 2016), because during partial melting, Nb, Ba and Rb behave incompatibly in amphibole (D^{Nb}_{amph}= 0·2; D^{Ba}_{amph}= 0·5 and D^{Rb}_{amph} = 0·3; le Roex et al., 1990; McKenzie and O'Nions, 1991; Adam et al., 1993; Dalpé and Baker, 1994), whereas Nb is incompatible (D^{Nb}_{Phlog} = 0·14; McKenzie and O'Nions, 1991) and Ba and Rb are strongly compatible in phlogopite (D^{phlog}_{Ba} = 2·9; D^{Rb}_{phlog} = 5·8; Adam et al., 1993). Therefore, the positive correlations between Ba and Rb versus Nb exhibited by Natash lavas (Fig.–8) are striking evidence in favour of an amphibole -bearing mantle source. Further evidence is provided by the relatively low potassium contents of the fractionation-corrected Natash basalts (5147 –7388 ppm), which fall within range of liquids formed by partial melting of an amphibole (pargasite)-bearing lherzolite (K

<20000 ppm, Späth et al. 2001). These contents are distinctly lower than those of partial melts formed from a phlogopite-bearing source (K>30000 ppm, Späth et al. 2001). The occurrence of–amphibole in the melting source region of Natash volcanics is in good agreement with its ubiquitous occurrence throughout the Arabian-Nubian lithosphere (e.g., Henjes-Kunst et al. 1990; Agrinier et al., 1993; Chazot et al.,1996, 1997; Kessel et al., 1997; Stein et al., 1997, Piccardo et al., 1993; Weinstein et al., 2006; Abu El-Rus,2007; Abu El-Rus and Rooney, 2017). The formation of amphibole in the lithosphere mantle of the Arabian-Nubian Shield is principally ascribed to the infiltration of volatile-rich metasomatic melts/fluids, significantly prior the melting event (e.g., Späth et al., 2001; Ma et al., 2011; Abu El-Rus and Rooney, 2017). The percolating metasomatic melts would create a continuum of phase assemblages within the lithosphere mantle ranging from anhydrous domains to hydrous, dominantly amphibole veins (e.g. Späth et al., 2001; Ma et al., 2011; Abu El-Rus and Rooney, 2017). Melting such heterogeneous mantle source would produce melt fractions exhibiting compositions that essentially depend on the contribution of each component to the melt (e.g., Späth et al., 2001; Pilet et al., 2008; McCoy-West et al., 2010; Sorbadere et al., 2013). Figure 9 shows that the most primitive Natash lavas can be reproduced by varying degrees of mixing between prevailing (>80%) melt fractions formed by up to 6 % of garnet-bearing lherzolite and subordinate melt fractions produced by 30-40% of garnet-bearing hornblendite. This estimation largely coincides with the experimental results of Pilet et al. (2008) which show that partial melts of hornblendite are highly Si-undersaturated, nephelinitic melts. The latters upon reactions with the ambient lherzolite can be turned to basanites and alkali basalts.

The metasomatic enrichment of the lithosphere mantle in the Arabian-Nubian Shield is principally ascribed to the release of fluids /melts either from subduction zones during the accretion of the Arabian-Nubian shield in Late-Neoproterozoic (subduction models; e.g., Thornber and Pallister, 1985; Abu El-Rus, 1991; Kröner et al., 1987; Henjes-Kunst et al., 1990; Brueckner et al., 1995, Stein et al., 1997; Shaw et al., 2007) or by a rising plume after the accretion of the Arabian-Nubian Shield (plume models; e.g., Stein and Hofmann, 1992; Baker et al., 1998; Beccaluva et al., 2009; Endress et al., 2011). Such metasomatic events would result in disturbance of the growth of ^{206}Pb and ^{207}Pb isotopes in the melting source which their ratio should remain constant if the system is closed. Therefore, the observed decoupling between^{206}Pb and ^{207}Pb isotopes in the most primitive Natash basalts suggests that the melting source should have been contaminated by small fractions of metasomatic fluids/melts with various Pb isotopic ratios prior to the eruption of the Natash volcanics. The relative timing of metasomatic enrichment can be therefore tentatively explored by calculating back isotope ratios through time until the ^{206}Pb and ^{207}Pb decoupling is removed. The important result of this modelling is that all Natash basaltic lavas become well aligned with a significant correlation coefficient (~ 0.9) only at ages older than 825 Ma (Fig. A5); a result that points to metasomatism occurred during the Late Proterozoic accretion of the Arabian-Nubian Shield (subduction model) rather than to a Phanerozoic rising plume as the most plausible cause for the disturbance of the Pb isotope system. This inference is in good agreement with Nd-Sr evidence provided by mantle xenoliths from Saudi Arabia, (Henjes-Kunst et al., 1990), peridotite bodies from Zabargad island (Brueckner et al. 1995), and clinopyroxene and amphibole megacrysts hosted in Quaternary basalts of

Arabian Peninsula (Altherr et al., 1990) that the isotopic heterogeneity of the lithospheric mantle in the Arabian-Nubian Shield originated during Pan-African times. Typical subduction zone hydrous fluids/melts are expected to have low Th abundances relative to U and Pb (Bailey and Ragnarsdottir, 1994), thus lowering $^{208}Pb/^{204}Pb$ relative to $^{207}Pb/^{204}Pb$ and $^{206}Pb/^{204}Pb$ values of lithospheric mantle: in contrast, carbonatite liquid have variable and often elevated $^{232}Th/^{204}Pb$ and $^{232}Th/^{238}U$ (Bell and Tilton, 2001).On this ground, the high initial $^{208}Pb/^{204}Pb$ values of the Natash basalt lavas (~39.5; Table 2) could indicate that carbonatite-like melts were the agents that enriched the mantle source of Natash mafic lavas. The positive correlation between Nb/Ta and Lu/Hf (Fig. A6) along with low Zr/Nb (3.4-4.2) observed in the most-primitive lavas provide additional evidence that the mantle source was overprinted by fluids/melts of carbonatitic affinity that most likely led to the slight Nb-excess observed in the continental basalts (e.g., Shaw et al., 2007; Pfänder et al., 2012). .This is consistent with the evidence for carbonatite metasomatism reported from the clinopyroxene remnants in mantle xenoliths ~~from~~ of the Natash basalts (Abu El-Rus et al., 2016).

b. Isotopic heterogeneity of the melting source

The almost linear variations in isotopic ratios (Fig. 5) and the wide range of several trace element ratios [e.g. $(Ce/Pb)_{corrected}$ =24-54 and $(P/Nb)_{corrected}$ =30-107; Table A7] in the Natash basalts likely result from heterogeneity of the melting source~~,~~ (Figs. 7, A4). The difference in the variation of $^{208}Pb/^{204}Pb$ and $^{207}Pb/^{204}Pb$ versus $2^{06}Pb/^{204}Pb$ isotope ratios (Fig. 5 c, d) rules out a simple binary melting source and therefore we explore a multi-component melting source model. On the triangular space defined by the relative

abundances of ^{206}Pb, ^{207}Pb, and ^{208}Pb isotopes (after Hanan et al., 1986, Fig. 10a), the Natash basalts form an array extending from Red Sea MORBs (both N- and E-type) and Ramad seamount array This array is bracketed by samples NAT-14 with the lowest, and NAT-12 with the highest, values of $^{207}Pb/^{204}Pb$. A third isotopic mantle component characterized by (low $^{87}Sr/^{86}Sr$ and εNd and low $^{206}Pb/^{204}Pb$ isotope ratios) can be detected by the displacement of the Natash sample array from the binary mixing lines between HIMU- and DM source compositions toward EMI mantle component in Figures 10 b,c. The involvement of EMI component can also be seen in the plotting of the Natash samples below the Red Sea MORBs and Ramad seamount array and extending towards EM composition in Figure 5. These constraints are consistent with three end-member components models which are usually called upon to explain the Nd-Sr-Pb isotope compositions of the intraplate volcanism in EARS (e.g., Barrat et al., 1990; Schilling et al. 1992; Deniel et al., 1994; Volker et al., 1997; Rooney et al., 2012). While these models agree on the presence of EM-like Pan-African continental lithosphere and MORB-depleted components in the melting source, they diverge as for the origin and significance of the Pb isotope enriched end-member. Schilling et al. (1992), Deniel et al. (1994) and Volker et al. (1997) invoke the existence of HIMU-like source component; Hanan and Graham (1996) and Rooney et al. (2012) in contrast, argue in favour of the role of a C component presents within Afar plume. Based on our evidence, the EM-DM-HIMU model of Schilling et al. (1992) is more consistent with the Sr-Nd-Pb-Hf signatures of Natash lavas. Furthermore, Figure 17 10 indicates that the multicomponent source is dominated by the HIMU end-member and that the mass fraction of the MORB depleted component predominates over the Pan-African lithosphere component.

Moreover, the continuous decreasing Sr isotopes and increasing Pb isotopes with the degrees of melting (Fig. ~~18~~ 11a, b) indicate the continuous contribution from HIMU-type in the generation of the Natash volcanic.

5.4 Melting within the lithospheric mantle

We used the melt compositions corrected for fractionation effects to estimate the potential temperature (Tp) and melting pressure (P_m) of source regions, as well as the melting fraction (*F*). Since all Natash basaltic lavas contain olivine and clinopyroxene phenocrysts, only the fractionation-corrected melts that involve an olivine and clinopyroxene addition on the liquid line of descent (LLD) are used to constrain the melting source. The calculations have been done following Putirka (2016), using the Excel spreadsheet available as electronic Appendix A1 on the MSA web site (http://www.minsocam.org/ MSA/AmMin/TOC/). Results are shown in Table (~~8~~ 4) and Figure ~~14~~ 12. The modelling suggests that the Natash basaltic lavas have derived from low degrees of partial melting ($F < 5\%$) at moderate potential temperatures (T_P) 1391 - 1425 ^{o}C and pressures of 2.0-2.6 GPa (at ~ 66- 86 km depth). These constraints imply that melting entirely occurred within lithospheric mantle that extends to 140 ± 40 km (e,g., Artemieva and Mooney, 2001; Stern, and Johnson, 2010). A lithospheric source is also supported by the presence of amphibole in the melting mantle source because amphibole is thermally unstable in both the convecting, asthenospheric upper mantle and in thermal mantle plumes (e,g,, Class and Goldstein, 1997; Späth et al., 2001; Pilet et al., 2008; Mc Coy-West et al., , 2010; Sorbadère et al., 2013; Abu El-Rus and Rooney, 2017).

The Natash lavas and their mantle xenoliths define a continuum array in term of pressure (depth), with a shift to higher temperatures for volcanic samples at a pressure of ~2 GPa. This deviation in the lithosphere geotherm is best explained by a thermal perturbation caused by a small hotspot (Garfunkel, 1989, Endress, et al., 2009) or by a hot asthenospheric lobe, channelled laterally from the South African Superplume (Endress et al., 2011) that has existed in the lower mantle since the breakup of supercontinent Pangaea at 175 Ma and possibly earlier (e.g., Burke et al., 2008,; Torsvik et al., 2008; Olson and Amit, 2015). Whatever the exact scenario, we suggest that lithospheric melting occurred essentially in response to heat flow from a thermally anomalous zone residing within the sub-lithospheric mantle.

5.5 Lithosphere-sublithosphere interaction: Geodynamic Implication

Modelling of Pb isotopic ratios back through time for the Natash basalts (Fig. A5) indicate a possible link between the metasomatism in the Pan-African lithosphere and the formation of juvenile crust during the early stages of Pan-Africa Orogeny. This implies that the fluids released from a hydrated subducted oceanic crust substantially metasomatized the overlying mantle wedge which coevally underwent partial melting, leading to island arc volcanism and formation of juvenile crust (Ryan and Langmuir 1993; Ishikawa and Nakamura 1994; Hoffman, 1997). The composition of the released fluids their quantities and the nature of percolation process (e.g. channels/veins, permeable flows associated chromatographic fractionation) would contribute substantially to the heterogeneity of the mantle wedge (e.g., (Bedini et al. 1997; Bodinier et al. 2004; Kessel et al., 2005; Hermann et al., 2006; Zack and John, 2007; John et al.,

2008; Mibe et al., 2011). Therefore, the mantle source of the Natash basaltic lavas can be tentatively regarded as a fossilized mantle wedge consisting of an ambient refractory DM component with interspersed EMI and HIMU components produced by the infiltration of melts/fluids released from subducted slab. The subtle variation in the amplitude of K-anomaly ($K^* = K_N/\sqrt{Ta_N}*La_N$) and melting pressure (Fig. 12 c) suggests some chemical stratigraphy of the lithosphere whereby melts produced at depth are slightly poorer in potassium than those produced at shallower levels. This vertical chemical zoning may be related to partial dehydration of the lower part of the amphibole-bearing lithosphere into clinopyroxene ± garnet assemblage due to conductive heating from underlying asthenosphere.

The emplacement of Natash volcanics at 90 Ma (e.g., El-Shazly and Krs, 1973; Hashad and El-Reedy, 1979; Ressetar et al., 1981) was coeval with the doming of Afro-Arabian Shield that initiated during Early-Late Cretaceous times (Coulter 1981; Crawfordet al., 1984; Hubbard et al., 1987) or alternatively with the long-term NW-trending extensional fracturing that initiated in Cretaceous times and continued till a N-S doming during the Miocene times. (Almond, 1986 a,b; Mohamed, 2001) . Whatever this doming was due to active or passive rifting, this implies the presence of a plume or upwelling asthenosphere–beneath the lithosphere some time before and/or during the eruption of the Natash volcanics. This plume or upwelling asthenosphere would act only as a source of heat triggering meting within the metasomatized continental lithosphere. The presence of this heat source is supported by the high thermal regime recorded by the mantle xenoliths brought to surface by Natash basalts. The steep geotherm calculated from the xenolith mineral assemblage corresponds to a surface heat flow of ~ 90 mWm^{-2}

(Abu El-Rus et al. 2016); a value significantly higher than the value of 40 mWm^{-2} characteristic the worldwide continental shields, (e,g, Gettings et al., 1986).

In summary, the major and trace elements and Sr-Nd-Pb-Hf isotope ratios of the Natash basaltic lavas indicate a two-stage evolution model for the melting within the mantle source whereby the Late-Proterozic lithosphere was refertilised and metasomatised by fluids and/or hydrous melts during Pan-African Orogeny and later on, i.e. during the doming or the extensional fracturing that preceded doming of the Afro-Arabian lithosphere in the late Cretaceous, underwent partial melting.

6. Conclusions

The Late Cretaceous Natash volcanics form a large intraplate magmatic province that borders the western margin of the Afro-Arabian dome in northeast Africa. We summarize our inferences from detailed chemical and isotopic analysis of the mafic lavas from this province as follows:

1- None of the basaltic lavas in Natash province represent a primary magma; they underwent polybaric fractional crystallization of various mineral assemblages formed by olivine ± clinopyroxene ± Cr-spinel. Plagioclase crystallized only at a late stage and at shallow levels.
2- Chemical and isotopic overprint of the Natash melts caused by assimilation of crust-derived materials seems negligible. Assimilation fractional crystallization (AFC) modelling is not able to re-produce the observed Sr-Nd-Pb-Hf signatures.

Furthermore, the positive correlation between SiO_2 and $^{143}Nd/^{144}Nd$ is difficult to reconcile with assimilation of continental crust. We interpret the variability of the isotopic composition of the Natash basalts ~~should be~~ as resulting from source heterogeneity and ~~to~~ melting degrees.

3- Semi-quantitative modelling of isotope ratios indicates the presence of Depleted Mantle (DM), Enriched Mantle (EM I) and High-μ mantle (HIMU) components within the melting source; the latter is predominant in the fingerprinting of the Natash basalts. Estimates of potential temperature (Tp) and melting pressures indicate that melting occurred within the lithospheric mantle. These calculations also suggest that the degree of partial melting was lower than 5%.

4- The presence of an amphibole signature in the composition of the Natash basalts indicates that the melting source underwent a metasomatic event before its melting in Late Cretaceous times. A possible link between metasomatism in the Pan-African lithosphere and formation of juvenile crust during the Pan-African Orogeny is suggested by time-integrated calculations from the Pb isotopic compositions of the mafic magmas.

5- Hydration and enrichment of the shallow mantle in response to interaction with fluids or hydrous melts released from the subduction zone during Pan-Africa Orogeny might represent important mechanism to create heterogeneity in the lithosphere mantle underneath the Afro-Arabian dome and its surrounding areas.

Acknowledgments

This work is a part of the research project entitled "*The evolution of lithospheric mantle beneath Nubian Shield: Evidence from mantle xenoliths from Egypt*" financed by Egypt – France Integrated Activities Program (IMHOTEP), contract 33 to Au El-Rus and Chazot. The field work Natash area in the south Eastern Desert was funded by Assiut Clermont-Ferrand and Pavia Universities. Laure Dosso is warmly thanked for performing the isotopic analyses. The manuscript has been benefit ~~by~~ from constructive comments and discussion ~~of~~ with Tanya Furman~~.~~ Comments by two anonymous reviewers and Editor Andrew Kerr contributed greatly to improving the manuscript.

References

Abu El-Rus, M. A. (2007) Plagioclase lherzolites from Zabargad Island, Red Sea, and their bearing on the evolution of lithospheric mantle beneath an embryonic ocean. ***The Fifth International Conference on the Geology of Africa*** Vol. 1, 181 – 213.

Abu El-Rus, M.A.; Chazot, G.; Vannucci, R.; Gahlan, H.A.; Boghdady, G.Y. and Paquette J.-L. (2016) Softening of sub-continental lithosphere prior rifting: Evidence from clinopyroxene chemistry in peridotite xenoliths from Natash volcanic province, SE Egypt**.** ***Journal of Volcanology and Geothermal Re***search 327, 84–98.

Abu El-Rus, M.A. and Rooney, T.O. (2017) Tertiary volcanic activity of the middle Egypt: A probe for asthenosphere-lithosphere interaction in northeast Africa. ***Chemical Geology,*** Chemical Geology 455, 282–303.

Adam, J., Green, T. H. and Sie, S. H. (1993). Proton microprobe determined partitioning of Rb, Sr, Ba, Y, Zr, Nb and Ta between experimentally produced amphiboles and silicate melts with variable F content. ***Chemical Geology*** 109, 29-49.

Agrinier, P., Mével, C., Bosch, F. and Javoy, M. (1993) Metasomatic hydrous fluids in amphibole peridotites from Zabargad Island (Red Sea). ***Earth and Planetary Science Letters*** 120, 187-205.

Albarède, F. (1992) How deep do common basalts form and differentiate? Journal of Geophysical Research 97, 10997–11009.

Almond, D.C. (1986a) The relation of Mesozoic-Cenozoic volcanism to tectonics in the Afro Arabian dome. ***Journal of Volcanology and Geothermal Research*** 28, 225-246.

Almond, D.C. (1986b) Geological evolution of the Afro-Arabian dome. ***Tectonophysics*** 131, 301-332.

Ariskin, A. A.; Barmina, G. S. and Frenkel M. Y. (1986) Simulating low-pressure tholeiite-magma crystallization at a fixed oxygen fugacity. ***Geochemistry International*** 24, 92–100.

Artemieva, I.M. and Mooney, W.D. (2001) Thermal thickness and evolution of Precambrian
lithosphere: a global study. ***Journal of Geophysical Research*** B106, 16387–16414.

Avni, Y.; Segev, A. and Ginat H. (2012) Oligocene regional denudation of the northern Afar dome: Pre- and syn-breakup stages of the Afro-Arabian plate. ***Geological Society of America Bulletin*** 124, 1871-1897

Bailey, J. A. and Ragnarsdottir, V. (1994) Uranium thorium solubilities in subduction zone fluids. ***Earth and Planetary Science Letters 124***, 119-129

Baker, J.; Chazot, G.; Menzies, M.A. and Thirlwall, M. (2002). Lithospheric mantle beneath Arabia: A Pan-African protolith modified by the Afar and older plumes, rather than a source for continental flood volcanism. In: Menzies, M. A., Klemper, S. L., Ebinger, C. & Baker, J. (eds) Volcanic Rifted Margins. ***Geological Society of America: Special Papers*** 362, 65-80.

Baldwin, S.L. and Ireland, T.R. (1995) A tale of two eras: Pliocene-Pleistocene unroofing of Cenozoic and late Archean zircons from active metamorphic core complexes, Solomon Sea, Papua New Guinea. ***Geology*** 23, 1023-1026.

Barrat, J.-A.; Jahn, B.-M., Fourcade, S. and Joron, J.L. (1993) Magma genesis in an ongoing rifting zone: The Tadjoura gulf (Afar area).***Geochimica Cosmochimica Acta*** 57, 2291-2302.

Barrat, J.A., Jahn, B.M.; Joron, J.L., Auvray, B. and Hamdi, H. (1990) Mantle heterogeneityin NE Africa: Evidencef rom Nd isotopicc ompositions and hygromagmaphilee lement geochemistryo f basalticr ocks from the Gulf of Tadjoura and Southern Red Sea regions. ***Earth and Planetary Science Letter***s 101,233-247.

Beccaluva, L.; Bianchini, G.; Natali, C. and Siena, F. (2009) Continental fl ood basalts and mantle plumes: A case study of the Northern Ethiopian Plateau. ***Journal of Petrology*** 50, 1377–1403.

Bedini, R.M., Bodinier, J.L., Dautria, J.M., and Morten, L., (1997) Evolution of LILE-enriched small melt fractions in the lithospheric mantle: A case study from the East African Rift. ***Earth and Planetary Science Letters*** 153, 67–83.

Bell K. and Tilton, G. R. (2001) Nd, Pb and Sr isotopic composition of East African carbonatites: evidence for mantle mixing and plume inhomogeneity. ***Journal of Petrology*** 42, 1927-1945.

Bertrand, H., Chazot, G.; Blichert-Toft, J. and Thoral, S. (2003) Implications of widespread high-μ volcanism on the Arabian Plate for Afar mantle plume and lithosphere composition. ***Chemical Geology*** 198, 47–61.

Bianchini, G.; Bryce, J.G; Blichert-Toft., J.; Beccaluva, L. and Natali, C. (2014) Mantle dynamics and secular variations beneath the East African Rift: Insights from peridotite xenoliths (Mega, Ethiopia). ***Chemical Geology*** 386, 49–58.

Bizimis, M., Salters, V.J.M., Dawson, J.B., 2003. The brevity of carbonatite sources in the mantle: evidence from Hf isotopes. ***Contributions to Mineralogy and Petrology*** 145, 281–300.

Blusztajn, J., Hart, S. R.; Shimizu, N. and McGuire, A. (1995) Trace element and isotopic characteristics of spinel peridotite xenoliths from Saudi Arabia. ***Chemical Geology*** 123, 53-65.

Bodinier, J.-L.; Menzies, M.A.; Shimizu, N.; Frey, F.A. and McPherson, E. (2004) Silicate, hydrous and carbonatemetasomatism at Lherz, France: contemporaneous derivatives of silicate melt harzburgite reaction. ***Journal of Petrology*** 45, 299–320.

Bosworth, W.; Huchon, P. and McClay, K. (2005) The Red Sea and Gulf of Aden Basins. ***Journal of African Earth Sciences*** 43, 334–378.

Bryan, W. B.; Thompson, G. and Ludden, J. N. (1981) Compositional variation in normal MORB from 228– 258N: Mid-Atlantic Ridge and Kane Fracture Zone. ***Journal of Geophysical Research***86, 11 815–11 836.

Burke, K., Steinberger, B., Torsvik, T. H., and Smethhurst, M. A. (2008). Plume generation zones at the margins of large low shear velocity provinces on the core-mantle boundary. ***Earth and Planetary Science Letters*** 265, 49–60.

Chazot, G., Menzies, M. and Harte, B. (1996) Determination of partition coefficients between apatite, clinopyroxene, amphibole, and melt in natural spinel lherzolites from Yemen: Implications for wet melting of the lithospheric mantle. ***Geochimica et Cosmochimica Acta*** 60, 423-437.

Chazot, G., Lowry D.; Menzies, M.A. and Mattey, D.P. (1997) Oxygen isotopic composition of hydrous and anhydrous mantle peridotites. ***Geochimica et Cosmochimica Acta*** 61, 161-169.

.

Class, C. and Goldstein, S. L. (1997). Plume-lithosphere interactions in the ocean basins: constraints from the source mineralogy. ***Earth and Planetary Science Letters*** 150, 245-260.

Class, C., and Le Roex, A. (2006), Continental material in the shallow oceanic mantle—How does it get there?, ***Geology*** 34, 129–132.

Corti, G. (2009) Continental rift evolution: From rift initiation to incipient break-up in the Main Ethiopian Rift, East Africa. ***Earth-Science Reviews*** 96, 1–53.

Cotton, J., Le Dez A. , Bau M. , Caroff M. , Maury R.C.; Dulski, P. and Brousse, R. (1995) Origin of anomalous rare-earth element and yttrium enrich,ments in sub aerially exposed basalts: evidence from French Polynesia**.** ***Chemical Geology*** 119, 115–138.

Coulter, D. H. (1981) Petrology and stratigraphy of the Wadi Natash Volcanics, Eastern Desert, Egypt. M.A. Thesis. Bryn Mawr College, Bryn Mawr, U.S.A.

Crawford, W.A. ,; Coulter, D.H. and Hubbard, H.B. (1984) The areal distribution, stratigraphy and major element chemistry of the Wadi Natash volcanic series, Eastern Desert, Egypt. ***Journal of African Earth Sciences*** 2, 119-128.

Dalpe, C. and Baker, D. R. (1994). Partition coefficients for rare-earth elements between calcic amphibole and Ti-rich basanitic glass at 1·5 GPa, 1100°C. ***Mineralogical Magazine*** 58A, 207-208.

Danyushevsky, L. V. and Plechovm, P. (2011) Petrolog3: Integrated software for modeling crystallization Processes. ***Geochemistry Geophysics Geosystems*** 12, 32pp, doi:10.1029/2011GC003516.

Deniel, C., Vidal, E.,. Coulon, C., Vellutini, E-J. and Piguet, P. (1994) Temporal evolution of mantle sources during continental rifting: The volcanism of Djibouti (Afar). ***Journal of Geophysical Research*** 99, 2853-2869.

De Paolo, D. J. (1981) Trace element and isotopic effects of combined wallrock assimilation and fractional crystallization. ***Earth and Planetary Science Letters*** 53, 189–202.

Ebinger, C.J. (2005) Continental breakup: the East African perspective. ***Astronomy and Geophysics*** 46, 2.16–2.21.

Ebinger, C.J.; Yemane, T.; Woldegabriel, G.; Aronson, J.L. and Walter, R.C., (1993) Late Eocene-recent volcanism and faulting in the southern main Ethiopian rift. ***Journal of the Geological Society*** London 150, 99-108.

Eissen, J.L.; Juteau, T.; Joron, J.L.; Dupre, B., Humler, E. and Al'Mukhamedov, A.I. (1989) Petrology and geochemistry of the basalts from the axial rift of the Red Sea at 18°N. ***Journal of Petrology*** 30, 791-839.

El-Gaby S., List F. K. and Tehrani R. (1988) Geology, evolution and metallogensis of the Pan-African belt in Egypt. In El-Gaby S. & Greiling R. O. (eds). ***The Pan-African Belt of Northeast Africa and Adjacent Areas***, Friedr. Vieweg. & Sohn Verlag, Braunschweig, pp. 17–68.

El-Shazly, E.M. and Krs, M., (1973) Paleogeography and paleomagnetism of the Nubian Sandstone, Eastern Desert of Egypt. ***Geologische Rundschau*** 62, 212-225.

Endress, C., Furman, T. and Abu El-Rus, M.A. (2009) Geochemistry of 24 Ma Basalts from Northeast Egypt: Implications for small-scale convection beneath the East African Rift System. American GeopysicalUnion (AGU). USA.

Endress, C.; Furman, T.; Abu El-Rus, M.A.A., and Hanan, B.B., (2011) Geochemistry of 24 Ma basalt from NE Egypt, in Van Hinsbergen, D.J.J., et al., eds., The Formation and Evolution of Africa: A Synopsis of 3.8 Ga of Earth History: Source components and fractionation history. ***Geological Society of London Special Publication*** 357,p. 265–283.

Ersoy, Y. and Helvacı, C. (2010) FC–AFC–FCA and mixing modeler: A Microsofts Excel & spreadsheet program for modeling geochemical differentiation of magma by crystal fractionation, crustal assimilation and mixing. ***Computers & Geosciences*** 36, 383–390.

Fitton, J.G. (1983). Active versus passive continental rifting; evidence from the West African rift system. ***Tectonophysics*** 94, 473 – 481.

Frey, F.A.; Green, D.H. and Roy, S.D. (1978) Integrated models of basalt petrogenesis: a study of quartz tholeiites to olivine melilitites from south eastern Australia utilizing geochemical and experimental petrological data. ***Journal of Petrology*** 19, 463–513.

Galer, S.J.G. and Abouchami, W. (1998) Practical application of lead triple spiking for correction of instrumental mass discrimination. ***Goldschmidt Conference****, Toulouse*.

Garfunkel, Z. (1989). Tectonic setting of Phanerozoic magmatism in Israel. ***Israel Journal of Earth Sciences*** 38, 51–74.

Green, D.H. (2015) Experimental petrology of peridotites, including effects of water and carbon on melting in the Earth's upper mantle. ***Physics and Chemistry of Minerals*** 42, 95–102.

Green, D. H. and Falloon, T. J. (2005). Primary magmas at mid-ocean ridges, 'hotspots', and other intraplate setting: Constraints on mantle potential temperature. In: Foulger, G. R., Natland, J. H., Presnall, D. C. & Anderson, D. L. (eds) "Plates, Plumes, and Paradigms". ***Geological Society of America***, ***Special Papers*** 388, 217-247.

Hanan, B. B. and Graham, D. W. (1996) Lead and helium isotope evidence from oceanic basalts for a common deep source of mantle plumes. ***Science*** 272, 991–995.

Hanan, B. B., Kingsley, R. and Schilling, J. G. (1986). Pb isotope evidence in the South Atlantic for migrating ridge^hotspot interactions. ***Nature*** 322, 137-144.
Hart, S.R. (1984). A large-scale isotope anomaly in the Southern Hemisphere mantle. ***Nature*** 309, 753-757.

Hart, S. R. and Davis, K. E. (1978) Nickel partitioning between olivine and silicate melt. ***Earth and Planetary Science Letters*** 40, 203-219.

Hashad, M.H. (1994) Geochemical characteristics and petrogenesis of phonolite-trachyte plugs associated with Wadi Natash volcanic rocks. ***Middle East Research Center Ain Shams University.***
Earth Science Series 8, 131-145.

Hashad, A.H. and El-Reedy, M.W.M. (1979). Geochronology of the anorogenic alkalic rocks, douth Eastern Desert, Egypt. ***Annals of the Geological Survey of Egypt*** 9, 81-101.

Hashad, A.H.; Hassan, M.A. and Aboul Gadayel, A.A. (1982) Geological and petrological study of Wadi Natash Late Cretaceous volcanics. ***Egyptian Journal of Geology*** 26, 19-37,

Henjes-Kunst, F.; Altherr, R. and Baumann, A. (1990) Evolution and composition of the lithospheric mantle underneath the western Arabian peninsula: constraints from Sr-Nd isotope systematics of mantle xenoliths. ***Contributions to Mineralogy and Petrology*** 105, 460 472.

Hermann, J.; Spandler, C.; Hack, A. and Korsakov, A.V., (2006) Aqueous fluids and hydrous melts in high-pressure and ultra-high pressure rocks: implications for element transfer in subduction zones. Lithos 92, 399–417.

Herzberg, C., and Asimow, P.D. (2015) PRIMELT3 MEGA.XLSM software for primary magma calcula¬tion: Peridotite primary magma MgO contents from the liquidus to the solidus. ***Geochemistry, Geophysics, Geosystems,*** doi: 10.1002/2014GC005631

Herzberg, C. and O'Hara, M. J. (2002). Plume associated magmas of Phanerozoic age.
Journal of Petrology 43, 1857-1883.

Hofmann A. W. (1997) Mantle geochemistry: the message from oceanic volcanism. ***Nature*** 385, 219-229.

Hubbard, H.B.; Wood, L.F. and Rogers, J.J. (1987). Possible hydration anomaly in the upper mantle prior to Red Sea rifting: Evidence from petrologic modelling of the Wadi Natash alkali basalt sequence of eastern Egypt. ***Geological Society America Bulletin*** 98, 92-98.

Hurai, V.; Paquette, J.L.; Huraiová, M. and Konečný, P. (2010) Age of deep crustal magmatic chambers in the intra-Carpathian back-arc basin inferred from LA-ICPMS U-Th-Pb dating of zircon and monazite from igneous xenoliths in alkali basalts. ***Journal of Volcanology and Geothermal Research*** 198, 275-287

Huismans, R.S.; Podladchikov, Y.Y. and Cloetingh, S. (2001) Transition from passive to active rifting: Relative importance of asthenospheric doming and passive extension of the lithosphere. ***Journal of Geophysical Research*** 106, 11,271-11,291.

Irvine, T.N. and Barager, W.R.A. (1971) A guide to the classification of the common volcanic rocks. ***Canadian Journal of Earth Sciences*** 8, 523-548.

Ishikawa, T. and Nakamura, E. (1994) Origin of the slab component in arc lavas from across-arc variation of B and Pb isotopes. ***Nature*** 370, 205-208.

Jackson, S.E.; Pearson, N.J.; Griffin, W.L. and Belousova, E.A. (2004) The application of laser ablation-inductively coupled plasma-mass spectrometry to in situ U–Pb zircon geochronology. ***Chemical Geology*** 211, 47-69.

John, T.; Klemd, R.; Gao, J. and Garbed-Schonberg, C.D. (2008) Trace-element mobilization in slabs due to non steady-state fluid–rock interaction: constraints from an eclogite facies transport vein in blueschist (Tianshan, China). ***Lithos*** 103, 1–24.

Kessel, R.; Navon, O. and Stein, M. (1997) Chromatographic metasomatism of the Arabian-Nubian lithosphere. ***Earth and Planetary Science Letters 152***, 75-91.
Kessel, R.; Schmidt, M.W.; Ulmer, P. and Pettke, T. (2005) Trace element signature of subduction-zone fluids, melts and supercritical liquids at 120–180 km depth. ***Nature*** 437, 724–727.

Khudeir, A. A.; Abu El-Rus; M. A., El-Gaby, S. and El-Nady, O. (2006) Geochemical and geochronological studies on the infrastructural rocks of Meatiq and Hafafit core complexes, Eastern Desert, Egypt. ***Egyptian Journal of Geology*** *50,* 190-214

Khudeir, A.A.; Abu El-Rus, M.A.; El-Gaby, S.; El-Nady, O. and Bishara, W.W. (2008) Sr–Ndisotopes and geochemistry of the infrastructural rocks in the Meatiq and Hafafit core complexes, Eastern Desert, Egypt: evidence for involvement of pre-Neoproterozoic crust in the growth of Arabian–Nubian shield. ***Island Arc*** 17, 90–108.

King, S.D., and Ritsema, J. (2000) African hotspot volcanism: Small-scale convection in the upper mantle beneath cratons. ***Science*** 290, 1137-1140.

Kogarko, L.N.; Asavin, A.M.; Barsikov, V.L.; Kolesov, G.M.; Kruchkova, O.I.; Polyakov, A.I.; Ramendik, G.I. (1984) A geochemical model for rare-earth fractionation in alkali-basalt series in South Atlantic islands. ***Geochemistry International*** 21, 27–39

Krienitz, M.-S.; Haase, K. M.; Mezger, K.; van den Bogaard, P.; Thiemann, V. and Shaikh-Mashail, M. A. (2009). Tectonic events, continental intraplate volcanism, and mantle plume activity in northern Arabia: constraints from geochemistry and Ar-Ar dating of Syrian lavas. ***Geochemistry, Geophysics, Geosystems*** 10, doi:10.1029/2008GC002254.

Kröner, A.; Stern, R.J.; Dawoud, A.S.; Compston, W. and Reischmann, T. (1987) The Pan-African continental margin in northeastern Africa; evidence from a geochronological study of granulites at Sabaloka, Sudan. ***Earth and Planetary Science Letters*** 85, 91–104.

Kröner A.; Todt W.; Hussein I. M.; Mansour M. and Rashwan, A. A. (1992) Dating of late Proterozoic ophiolites in Egypt and the Sudan using the single grain zircon evaporation technique. ***Precambrian Research*** 59, 15–32.

Lassiter, J.; C., Blichert-Toft, J.; Hauri, E. H. and Barsczus, H. G. (2004) isotope and trace element variations in lavas from Raivavae and Rapa, cook-austral islands: constraints on the nature of HIMU- and EM-mantle and the origin of mid-plate volcanism in French Polynesia. ***Chemical Geology*** 202, 115-138.

Le Bas, M.J.; Le Maitre, R.W.; Streckeisen, A and , Zanetin, B. (1986) A chemical classification of volcanic rocks based on the total alkalis-silica diagram. ***Journal of Petrology*** 27, 745-750.

Leeman, P. and Fitton, J.G. (1989) Magmatism associated with lithospheric extension: introduction, ***Journal of Geophysical Research*** 94, 7682-7684.

le Roex, A. P. and Watkins, R. T. (1990). Analysis of rare-earth elements in geological samples by gradient ion chromatography: an alternative to ICP and INAA. ***Chemical Geology*** 88, 151-162.

Lutz, T.M.; Foland, K.A.; Faul, H. and Srogi, L.A. (1988) The strontium and oxygen isotopic record of hydrothermal alteration of syenites from the Abu Khruq complex, Egypt. ***Contributions to Mineralogy and Petrology*** 98, 212-223.

McKenzie, D. and O'Nions, R. K. (1991). Partial melt distributions from inversion of rare earth element concentrations. *Journal of Petrology* **32**, 1021-1091.

Ma, G.S.-K., Malpas, J., Xenophontos, C., Chan and G.H.-N. (2011) Petrogenesis of Latest Miocene- Quaternary continental intraplate volcanism along the Northern Dead Sea fault system (Al Ghab-HomsVolcanic field), western Syria: evidence for lithosphere asthenosphere interaction. ***Journal of Petrology*** 52, 401–430.

Mackenzie, G., Thybo, H., Maguire, P. (2005) Crustal velocity structure across the Main Ethiopian Rift: results from 2-dimensional wide-angle seismic modelling. ***Geophysical Journal International 162,*** 994–1006.

McCoy-West, A.J., Baker, J.A., Faure, K., Wysoczansk, R., 2010. Petrogenesis and origins of
Mid-Cretaceous continental IntraplateVolcanism in Marlborough, New Zealand: implications for the long-lived HIMU magmatic mega-province of the SW Pacific. ***Journal of petrology*** 51, 2003–2045.

Madani, A.A. (2000) "*Geological studies and remote sensing applications on Wadi Natash volcanics, Eastern Desert, Egypt*". ***Ph.D. Thesis, Faculty of Science, Cairo University***.

McDonough, W. F. and Sun, S.-S. (1995). The composition of the Earth. ***Chemical Geology*** 120, 223–253.

McKenzie, D.P. and Bickle, M.J. (1988) The volume and composition of melt generated by extension of the lithosphere. ***Journal of Petrology 29***, 625-679.

Mibe, K.; Kawamoto, T.; Matsukage, K.N.; Fei, Y. and Ono, S. (2011) Slab melting versus slab dehydration in subduction-zone magmatism. ***Proceedings of the National Academy of Sciences*** 108, 8177–8182.

Mohamed, F.H. (2001) The Natash alkaline volcanic field, Egypt: geochemical and mineralogical inferences on the evolution of a basalt to rhyoliteeruptive suite. ***Journal of Volcanology and Geothermal Research*** 105, 291- 322.

Morimoto, N.; Fabries, J.; Ferguson, A. K.; Ginzburg, I.V; Ross, M.; Seifert, F.A.; Zussman, J.; K. Aoki, K. and Gottardi, G.(1988) Nomenclature of pyroxenes. ***American Mineralogist 7 3, 11 2 3- 1133.***

Müller, W.; Shelley, M.; Miller, P. and Broude, S. (2009) Initial performance metrics of a new custom-designed Ar Fexcimer LA-ICPMS system coupled to a two-volume laser-ablation cell. ***Journal of Analytical Atomic Spectrometry*** 24, 209-214.

Nasir, S. and Rollinson, H. (2009). The nature of the subcontinental lithospheric mantle beneath the Arabian Shield: mantle xenoliths from southern Syria. Elsevier. ***Precambrian Research*** 172, 323-333.

Nathan, H. D., and Van Kirk, C. K. (1978) A model of magmatic crystallisation, ***Journal of Petrology*** 19, 66–94.

Neumann, E.-R.; Abu El-Rus, M. A.; Tiepolo, M.; Ottolini, L., Vannucci, R. and Whitehouse, M. (2015) Serpentinization and Deserpentinization Reactions in the Upper Mantle beneath Fuerteventura Revealed by Peridotite Xenoliths with Fibrous Orthopyroxene and Mottled Olivine. ***Journal of Petrology*** 56,3-31.

Nielsen, R. L., and Dungan, M. A. (1983) Low pressuremineral- melt equilibria in natural anhydrous mafic systems. ***Contributions to Mineralogy and Petrology*** 84, 310–326.

Nimis, P. (1995) A clinopyroxene geobarometer for basaltic systems based on crystal-structure modeling. ***Contributions to Mineralogy and Petrology*** 121, 115-125.

Nimis, P. and Ulmer, P. (1998) Clinopyroxene geobarometry of magmatic rocks. 1. An expanded structural geobarometer for an- hydrous and hydrous, basic and ultrabasic systems. ***Contributions to Mineralogy and Petrology*** 133: 314-327.

Niu, Y. and O'Hara, M.J. (2007) Global correlations of ocean ridge basalt chemistry with axial depth: a new perspective. ***Journal of Petrology*** 49, 633–644.

O'Hara, M.J. (1968) Are ocean floor basalts primary magma? ***Nature*** 220, 683–686.

Olson, P. and Amit, H. (2015) Mantle superplumes induce geomagnetic superchrons. ***Frontiers in Earth Science,*** 3, doi: 10.3389/feart.2015.00038

O'Nions, R.K.; Hamilton P.J. and Evensen, N.M. (1977) Variations in $^{143}Nd/^{144}Nd$ and $^{87}Sr/^{86}Sr$ in oceanic basalts. ***Earth and Planetary Science Letters*** 34, 13-22.

Pfänder, J. A.; Jung, S., Münker, C; Stracke, A. and Mezger, K. (2012) A possible high Nb/Ta reservoir in the continental lithospheric mantle and consequences on the global Nb budget Evidence from continental basalts from Central Germany**.** ***Geochimica et Cosmochimica Acta*** 77 232–251.

Paquette, J.L. and Tiepolo, M. (2007) High resolution (5 μm) U-Th-Pb isotopes dating of monazite with excimer laser ablation (ELA)-ICPMS. ***Chemical Geology*** 240, 222-237.

Paquette, J.L.; Piro, J.L.; Devidal, J.L.; Bosse, V. and Didier, A. (2014) Sensitivity enhancement in LA-ICP-MS by N2 addition to carrier gas: application to radiometric dating of U-Th-bearing minerals. ***Agilent ICP-MS journal*** 58, 4-5.

Pilet, S., Baker, M.B. and Stolper, E.M. (2008) Metasomatized litho sphere and the origin of alkaline lavas. ***Science*** 320, 916–919.

Piccardo, G. B.; Rampone, E. ; Vannucci, R.; Shimizu, N.; Ottolini, L. and Bottazzi, P. (1993) Mantle processes in the sub-continental lithosphere: the case study of the rifted sp-lherzolites from Zabargad (Red Sea). ***European Journal of Mineralogy*** 5 1039 – 1056.

Putirka, K. (2016) Rates and styles of planetary cooling on Earth, Moon, Mars, and Vesta, using new models for oxygen fugacity, ferric-ferrous ratios, olivine-liquid Fe-Mg exchange, and mantle potential temperature. ***American Mineralogist*** 101, 819–840.

Putirka, K. D.; Mikaelian, H.; Ryerson, F. and Shaw, H. (2003) New clinopyroxene-liquid thermobarometers for mafic, evolved, and volatile-bearing lava compositions, with application to lavas from Tibet and the Snake River Plain, Idaho. ***American Mineralogist*** 88, 1542–1554.

Radwan, A.H.A. and Issawy, E.A. (2006) Integrated lithospheric modelling in the Red Sea area. ***Contributions to Geophysics and Geodesy*** 36, 383-364.
Rayan, J.G. and Langmuir, C.H. (1993) The systematic of boron abundances in young volcanic rocks. 57, ***Geochimica et Cosmochimica Acta***1489-1498.

Ressetar, R.; Nairn, A.E.M. and Monrad, J.R., (1981) Two phases of cretaceous-Tertiary magmatism in the Eastern Desert of Egypt: Paleomagnetic, chemical and K-Ar evidence. ***Tectonophysics*** 73, 169-193.

Roeder, P.L. and Emslie, R.F., (1970) Olivine-liquid equilibrium. ***Contributions to Mineralogy and Petrology*** 19, 275–289.

Rooney, T.O. (2017) The Cenozoic magmatism of East-Africa: Part I — Flood basalts and pulsed magmatism, ***Lithos*** 286-287, 264-301.

Rooney, T.O.; Bastow, I. and Keir, D. (2011) Insights into extensional processes during magma assisted rifting: Evidence from aligned scoria cones. ***Journal of Volcanology and Geothermal Research*** 201 83–96.

Rooney, T.O.; Hanan, B.B.; Graham, D.W.; Furman, T.; Blichert-Toft, J., and Schilling, J. G., (2012) Upper mantle pollution during Afar plume– continental rift interaction: ***Journal of Petrology***v. 53, 365–389.

Salters, V. J. M.; Mallick, S; Hart, S. R.; Langmuir, C. H. and Stracke A. (2011) Domains of depleted mantle: new evidence from hafnium and neodymium isotopes. ***Geochemistry Geophysics Geosystems*** 12, D.O.I. 10.1029/2011GC003617.

Salters, V. J. M. and White W. M.(1998) Hf isotope constraints on mantle evolution. ***Chemical Geology 145***, 447-460

Sato, H. (1977) Nickel content of basaltic magmas: identification of primary magmas and a measure of the degree of olivine fractionation. ***Lithos*** 10, 113-120.

Schilling, J.-G.; Kingsley, R.H.; Hanan, B.B. and McCully, B.L. (1992) Nd-Sr-Pb variations along the Gulf of Aden: Evidence for Afar mantle plume--continental lithosphere interaction. ***Journal of Geophysical Research*** 97, 10927-10966.

Sisson, T.W. and Grove, T.L. (1993) Experimental investigations of the role of H_2O in calc-alkaline differentiation and subduction zone magmatism. ***Contributions to Mineralogy and Petrology*** 113, 143-166.

Sgualdo, P.; Aviado , K.; Beccaluva, L.; Bianchini, G.; Blichert-Toft , J.; Bryce , J.G.; Graham, D.W.;Natali, C. and Siena, F. (2015) Lithospheric mantle evolution in the Afro-Arabian domain: Insights from Bir Ali mantle xenoliths (Yemen). ***Tectonophysics*** 650, 3–17.

Shaw, J. E.; Baker, J.A.; KENT, J.R.; Ibrahim, K.M. and Menzies, M.A. (2007) The Geochemistry of the Arabian Lithospheric Mantle- a Source for intraplate volcanism? ***Journal of Petrology*** 48, 1495-1512.

Shaw, J. E.; Baker, J. A.;Menzies, M. A.; Thirlwall, M. F. and Ibrahim, K. M. (2003). Petrogenesis of the largest intraplate volcanic field on the Arabian Plate (Jordan): a mixed lithosphere-asthenosphere source activated by lithospheric extension. ***Journal of Petrology*** 44, 1657-1679.

Sleep, N.H., (1996) Lateral flow of hot plume material ponded at sublithospheric depths. ***Journal of Geophysical Research*** 101, 28,065 -28,083.

Späth, A., le Roex, A. P. and Duncan, R. A. (1996). The geochemistry of lavas from the Comores Archipelago, western Indian Ocean: Norry, petrogenesis and mantle source region characteristics. ***Journal of Petrology*** 37, 961-991.

Späth, A.; Le Roex, A.P. and Opiyo-Akech, N. (2001) Plume–Lithosphere Interaction and the Origin of Continental Rift-related Alkaline Volcanism—the Chyulu Hills Volcanic Province, Southern Kenya. ***Journal of Petrology*** 42, 765-787.

Stein, M. and Hofmann, A. W. (1992) Fossil plume head beneath the Arabian lithosphere? ***Earth and Planetary Science Letters*** 114, 193-209.

Stein, M., Navon, O., and Kessel, R., (1997) Chromatographic metasomatism of the Arabian Nubian lithosphere. ***Earth and Planetary Science Letters*** 152, 75–91.

Stern, R.J. and Johnson, P. (2010) Continental lithosphere of the Arabian Plate: A geologic, petrologic, and geophysical synthesis. ***Earth-Science Reviews*** 10, 29–67.

Stern, R.J.; Kröner, A. and Rashwan, A.A. (1991) A late Precambrian (~ 710 Ma) high volcanicity rift in the southern Eastern desert of Egypt. ***Geologische Rundchau*** 80, 155-170.

Sun, S.-S. and McDonough, W. F. (1989) Chemical and isotopic systematics of oceanic basalts: implications for mantle composition and processes. In: Saunders, A. D. & Norry, M. J. (eds) Magmatism in the Ocean Basins. ***Geological Society, London, Special Publications*** 42, 313-345

Teklay, M.; Scherer, E. E.; Mezger, K. and Danyushevsky L. (2010) Geochemical characteristics and Sr–Nd–Hf isotope compositions of mantle xenoliths and host basalts from Assab, Eritrea: for the composition and thermal structure of the lithosphere beneath the Afar Depression. ***Contributions to Mineralogy and Petrology 159.731***–751.

Tera, F. and Wasserburg, G.J. (1972) U–Th–Pb systematics in three Apollo 14 basalts and the problem of initial Pb in lunar rocks. ***Earth and Planetary Science Letters***14,281–304.

Thirlwall, M. F. (1997) Pb isotopic and elemental evidence for OIB derivation from young HIMU mantle. ***Chemical Geology*** 139, 51–74.

Thybo, H. and Artemieva, I.M. (2013) Moho and magmatic underplating in continental lithosphere. ***Tectonophysics*** 609, 605–619.

Thybo, H. and Nielsen, C.A. (2009) Magma-compensated crustal thinning in continental rift zones. ***Nature*** 457, 873–876.

Tormey, D. R.; Grove, T. L. and Bryan, W. B. (1987) Experimental petrology of normal MORB near the Kane Fracture Zone: 228–258N, mid-Atlantic ridge. ***Contributions to Mineralogy and Petrology*** 96, 121–139.

Thornber, C.R. and Pallister, J.S. (1985) Mantle xenoliths from northern Saudi Arabia. ***EOS Transactions American Geophysical Union*** 66, 393.

Turcotte, D.L. (1989).Dynamics of recycling. In : S.R. Hart and L. Giilen Torsvik, T. H., Smethurst, M. A., Burke, K., and Steinberger, B. (2008). Long-term stabilityin deep mantle structure: evidence from the 300Ma Skagerrak Centered Large Igneous Province (the SCLIP). ***Earth and Planetary Science Letters*** 267, 444–452.

van Achterbergh, E.; Ryan, C.G.; Jackson, S.E. and Griffin, W.L. (2001) Data reduction software for LA-ICP-MS. In Laser ablation-ICPMS in the earth science. P. Sylvester ed. ***Mineralogical Association of Canada*** 29, 239-243.

Vidal, R; Deniel, C.; Vellutini, EG.; Piguet, R.; Coulon, C.; Vincent and J., Audin, J. (1991) Changes of mantle sources in the course of a rift evolution: The Afar case. ***Geophysical Research Letters***18, 1913-1916.

Volker, F.; Altherr, R.; Jochum K-P. and McCulloch M. T. (1997) Quaternary volcanic activity of the southern Red Sea: new data and assessment of models on magma sources and Afar plume lithosphere interaction. ***Tectonophysics*** 278, 15-29.

Volker, F., McCulloch, M.T., Altherr, R. (1993) Submarine basalts from the Red Sea: New Pb, Sr, and Nd isotopic data. ***Geophysical Research Letters*** 20, 927-930.

Walter, M. J. (1998). Melting of garnet peridotite and the origin of komatiite and depleted lithosphere. ***Journal of Petrology*** 39, 29-60.

Weaver, B.L.; Wood, D.A.; Tarney, J. and Joron, J.L. (1987) Geochemistry of ocean island basalts from the South Atlantic, Ascension, Bouvet, St. Helena, Gough and Tristan da Cunha. In: J.G. Fitton and B.G.J. Upton (Eds.) "alkaline igneous rocks" ***Geological Society, London, Special Publications*** 30, 253-267.

Weinstein, Y.; Navon, O.; Altherr, R. and Stein, M. (2006) The role of lithospheric mantle heterogeneity in the generation of Plio- Pleistocene alkali basaltic suites from NW Harrat Ash Shaam (Israel). ***Journal of Petrology*** 47, 1017–1050.

Wiedenbeck, M.; Allé, P.; Corfu, F.; Griffin, W.L.; Meier, M.; Oberli, F.; von Quadt, A.; Roddick, J.C. and Spiegel, W., (1995)Three natural zircon standards for U-Th-Pb, Lu-Hf, trace element and REE analyses. ***Geostandards Newsletter*** 19, 1-23.

Willbold, M. and Stracke, A. (2006) Trace element composition of mantle end-members: implications for recycling of oceanic and upper and lower continental crust. ***Geochemistry Geophysics Geosystems*** 7, doi:10.1029/2005GC001005

White, R.S.; Spence, G.D.; Fowler, S.R.; MCKenzie, D.P.; Westbrook, G.K. and Bowen, A.N. (1987) Magmatism at rifted continental margins, ***Nature*** 330, 439-444.

White,W.M.; Albarède, F. and Telouk, P. (2000) High-precision analysis of Pb isotope ratios by multi-collector ICP-MS. ***Chemical Geology*** 167, 3–4, 257–270.

Zack, T. and John, T. (2007) An evaluation of reactive fluid flow and trace element mobility in subducting slabs. ***Chemical Geology*** 239, 199–216.

Ziberna, L.; Klemme, S. and Nimis, P. (2013) Garnet and spinel in fertile and depleted mantle: insights from thermodynamic modelling. ***Contributions to Mineralogy and Petrology*** 166, 411-421.

Zindler, A. and Hart, S.R. (1986) Chemical geodynamics. ***Annual Review of Earth and Planetary Sciences***14, 493–571.

Text of Figures:

Figure 1: (a) Sketch map of Afro-Arabian dome (outlined by dashed line) and its surrounding area (modified after Almond 1986a) showing the location of the Natash volcanic province. The figure also shows the distribution of the main four within-plate magmatism types in Arabia and NE Africa (Almond 1986a,b): (1) Late Cretaceous - Oligo-Miocene volcanism of mainly transitional affinity (Ethiopian and Yemen trap series stippled areas), (2) MORB tholeiites that form the south Red Sea and Gulf of Aden basins, (3) Miocene alkaline volcanism eruptions associated with uplift producing the Afro-Arabian Dome (black areas) and (4) Alkaline volcanism of the East Sahara swell and Western Desert basin to the west of the Afro-Arabian Dome. Diagonal shading area represents stretched continental crust and MORB occurrences (SCC+MORB) (b) Geologic map of the Wadi Natash volcanics showing the distribution of the various volcanic units within the province (modified after Crawford et al., 1984).

Figure 2: Composition of Natash lavas on the SiO_2 versus total alkalis (TAS) diagram after Le Bas et al. (1986). The stippled area shows the composition range of the entire succession within the Natash volcanic province (data from Mohamed 2001). The boundary line between the alkaline and subalkaline fields is after Irvine and Baragar (1971).

Figure 3: Bivariate plots of selected major (wt. %) and trace elements (ppm) versus Mg# for alkali olivine basalts, trachybasalts and basanites lavas from the Natash volcanics province. Open circles are the present work data whereas filled diamonds are data from Mohamed (2001).

Figure 4: Primitive- mantle normalized patterns for moderately to highly incompatible elements for alkali olivine basalt, trachybasalt and basanites from the Natash volcanic province. Gray fields are the fractionation-corrected melts (in the range of 0.68-0.72 mg# buffered at fO_2 corresponding to Fe_2O_3/TiO_2 values between 0.5 and 1.0 (see text for details). The fractionation-corrected compositions which are not consistent with primary melt compositions (e.g. calculated melts for sample NAT-14) are not included in the grey field. Average compositions of N-type and E-type MORB and oceanic island basalts (OIB) are reported for comparison (data from Sun and McDonough, 1989). Normalization values are from McDonough and Sun (1995).

Figure 5: (a) $^{87}Sr/^{86}Sr$ vs $^{143}Nd/^{144}Nd$, (b) εNd vs εHf, (c) $^{207}Pb/^{204}Pb$ vs $^{206}Pb/^{204}Pb$ and (d) $^{208}Pb/^{204}Pb$ vs $^{206}Pb/^{204}Pb$ for the Natash basaltic lavas. Representative points and fields reported for comparison are: basalts from the Red Sea axial trough (i.e. Red Sea MORB, open diamond) – Ramad Seamount with HIMU-type signatures (data from

Eissen et al. 1989; Volker et al., 1993; 1997), the Sheba Ridge MORB-(Gulf Aden, data from Schilling et al. 1992 for Sr, Nd and Pb isotopes and Rooney et al., 2012 for Hf isotopes), the Afar plume volcanics in a, c and d (data from Vidal et al., 1991; Deniel et al., 1994 in a, b,d), the Saudi Arabia intraplate basalts (data from Altherr et al., 1990), the Afro-Arabian plate basalts (data from Bertrand et al. 2003 and Endress et al., 2011), the Arabian-Nubian lithospheric mantle (i.e. cpx separates from mantle xenoliths: data from Henjes-Kunst et al., 1990; Stein et al., 1993; Blusztajn et al., 1995; Baker et al., 1998, 2002; Shaw et al., 2007; Nasir and Rollinson, 2009; Bianchini et al., 2014; Sgualdo et al., 2015), the East Sahara Swell and Western Desert basin intraplate basalts (data from Lucassen et al., 2008). Indian and Pacific MORBs, Sabaha Ridge and Main Ethiopian rift lavas in b are from Rooney et al. (2012). Mantle end-member components DMM, BSE, HIMU, EM1 and mixing lines in a are from Zindler and Hart, (1986); mantle end-member DM and Afar plume, C mantle and the mantle array (dashed line) in b are from Rooney et al. (2012). NHRL (Northern Hemisphere Reference Line) is from Hart (1984).Open and filled circles are the present-day isotopic ratios and the initial isotopic ratios at 90 Ma for Natash mafic lavas, respectively.

Figure 6: Major and trace element composition of the fractionation-corrected Natash lavas calculated using the Petrolog software. (a) Ni (ppm) vs Mg#. Solid and dashed lines are fractionation paths buffered at fO_2 corresponding to Fe_2O_3/TiO_2 values comprised between 0.5 and 1.0 respectively. The gray field shows the primary melt compositions (Mg# =68-72 and Ni =300-500 ppm, e.g. Herzberg and O'Hara, 2002; Green and Falloon, 2005). (b, c) Plots showing the conservative behavior of the incompatible trace element ratios during fractional crystallization. Bars represent the ranges of ratios in the

fractionation-corrected melts calculated to 68-72 Mg# and buffered at fO_2 conditions corresponding to Fe_2O_3/TiO_2 values from 0.5 and 1.0 (upper and lower values are illustrated by filled and open symbols, respectively).

Figure 7: (A,B) Assimilation–fractional crystallization (AFC; DePaolo, 1981) and (C) bulk mixing calculations illustrating the possible effects of assimilation of Late Proterozoic lower continental crust from the Afro-Nubian Shield. The crust component used in the modelling has the average composition of the mafic granulites form western Saudi Arabia (McGuire and Stern 1993) and from Zabargad Island (Brueckner et al. 1995), namely Sr = 538 ppm, Nd = 9.45 ppm, $^{87}Sr/^{86}Sr$ = 0.703363 and $^{143}Nd/^{144}Nd$ = 0.512620. The starting composition used in modelling is the composition of the fractionation-correct melts of the most and least primitive samples NAT-13 and NAT-14 respectively. Sample NAT-13 exhibits Sr= 506 ppm, Nd= 33 ppm, $^{87}Sr/^{86}Sr$ = 0.703054 and $^{143}Nd/^{144}Nd$ = 0.512653. Samples NAT-14 exhibits Sr= 460 ppm, Nd= 30 ppm**,** $^{87}Sr/^{86}Sr$ = 0.702858 and $^{143}Nd/^{144}Nd$ = 0.512761. The ‘‘r’’ values in A and B are the relative ratio of assimilated material to crystallized melt, whereas the small tricks (F) on the AFC trajectories are the fraction of the remaining melt during cooling of the magma. The small tricks on the trajectory in C are the proportions of degree of bulk mixing between the starting composition NAT-13 and lower crust mafic granulite. Open and filled circles are corrected melt compositions calculated under oxidizing and reducing conditions, respectively. The calculations were performed using Excel & spreadsheet FC–AFC–FCA and mixing modeler of Ersoy and Helvaci (2010). More details are present in Appendix E.

Figure 8: Plots showing the positive correlation of Rb and Ba with Nb (data in ppm) in the fractionation-corrected melts of the Natash mafic flows. Open and filled circles are corrected melt compositions calculated under oxidizing and reducing conditions, respectively

Figure 9: The fractionation-corrected melts of the most primitive Natash lavas compared to the non-modal batch melting trajectories (after Ma et al., 2011) of a fertile garnet-bearing lherzolite (sample KR4003 of Walter, 1998) and a hornblendite metasomatic vein (AG4 of Pilet et al., 2008) as starting materials. The kink in the melting trajectories of garnet- bearing hornblendite results from complete exhaustion of amphibole; beyond this point the melting mode of the residual ‘‘pyroxenite’’ vein is assumed. Ticks on the melting trajectories represent the degree of melting (*F*). Clearly, neither melting of garnet- bearing lherzolite nor melting of garnet-bearing hornblendite veins can alone reproduce the trace element composition of the Natash lavas. The Natash samples fall between the two melting trajectories and are best interpreted as products of varying degrees of mixing of prevailing (>80%, tricks along the dashed line) melt fractions formed by up to 6% of garnet-bearing lherzolite melting and subordinate melt fractions resulted from 30-40% melting of garnet-bearing hornblendite veins. Open and filled circles are corrected melt compositions calculated under oxidizing and reducing conditions, respectively. Primitive mantle normalizing values are from Sun and McDonough (1989).

Figure 10: (a) The Natash mafic lavas plotted on the triangular Pb isotope plot of the relative abundances of ^{206}Pb, ^{207}Pb, and ^{208}Pb (after Hanan et al., 1986). The lavas define

a quasi-linear trend passing through the composition of the Afar plume (A1) and extending to higher $^{206}Pb/^{204}Pb$ ratios towards the HIMU component. Plotted for comparison are basalts from the Red Sea axial trough (.e. Red Sea MORB, open diamond) – Ramad Seamount with HIMU-type signature (data compiled from Eissen et al. 1989; Volker et al., 1993; 1997). End members: DM, depleted mantle ($^{206}Pb/^{204}Pb$=17·5; $^{207}Pb/^{204}Pb$=15·3, $^{208}Pb/^{204}Pb$=36.2) and Pan African, Pan-African lithosphere ($^{206}Pb/^{204}Pb$=17·9; $^{207}Pb/^{204}Pb$=15·8, $^{208}Pb/^{204}Pb$=39·8) are from Schilling et al. (1992) and Rooney et al. (2012). Whereas Schilling (1992) considered the Afar plume end-member (A1) of HIMU-like composition ($^{206}Pb/^{204}Pb$=20.8, $^{207}Pb/^{204}Pb$=15·7, $^{208}Pb/^{204}Pb$=40.10). Hanan and Graham (1996) considered that the composition of Afar plume lies within the range of compositions for the common component 'C' with average Pb-isotopic of $^{206}Pb/^{204}Pb$=19.5; $^{207}Pb/^{204}Pb$=15·6 and $^{208}Pb/^{204}Pb$=39.2 (A1, Rooney et al., 2012). Fields of HIMU component and Afar plume are from Rooney et al., (2012). The ternary grid interval is 0.25%. $^{87}Sr/^{86}Sr$ vs $^{206}Pb/^{204}Pb$ (b) and $^{143}Nd/^{144}Nd$ vs $^{206}Pb/^{204}Pb$ (c) plots for the Natash mafic lavas. Data sources for calculation binary mixing lines calculations between different end-member components are as in (A). HIMU, DMM, EMI and EMII end-member mantle components are after (Zindler and Hart, 1986). The calculations are carried out using the element concentrations and isotopic ratios provided in Appendix G. Open circles are present-day ratios, while filled circles are initial ratios at ~90 Ma.

Figure 11: (a, b) Estimated melting fraction vs $(^{87}Sr/Sr^{86})_i$ and $(^{206}Pb/^{204}Pb)_i$, respectively. (c) Melting pressure vs the K-anomaly ($K^* = K_N/\sqrt{Ta_N}*La_N$). Only fractionation-corrected melts that exhibit primary characters (Mg# > 68% and Ni > 300ppm) are

shown. Open and filled circles are corrected melt compositions calculated under oxidizing and reducing conditions, respectively.

Figure 12: Potential temperatures (T_P) - melting pressure(P_M) estimates for the melting source as calculated from the fractionation-corrected melts for the Natash mafic lavas. Solidi for mid-ocean ridge basalt (MORB) pyrolite (fertile mantle, MPY), Tinaquillo lherzolite compositions (depleted mantle, TQ) and Hawaiian pyrolite (enriched mantle, HPY) stability fields (Green and Falloon, 2005; Green 2015). Stability fields for plagioclase, spinel, and garnet-lherzolite mineralogy (dashed lines) are for the Hawaiian pargasite pyrolite (Green and Falloon, 2005; Green 2015), whereas dot lines represent the coexisting field of garnet and spinel for mid-oceanic basalt pyrolite after (Ziberna et al., 2013). Dehydration solidus is for the Hawaiian pargasite- pyrolite composition (Green and Falloon, 2005; Green 2015). Stippled area represents the depths of base of the crust located on both sides of the Red Sea (28-33 km; Radwan and Issawy, 2006). Stars are the equilibrium P-T for mantle xenoliths enclosed within Natash basic flows whereas circles are Tp and Pm for the calculated primary melts for Natash basic flows (Open and filled circles are corrected melt compositions calculated under oxidizing and reducing conditions, respectively).

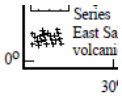

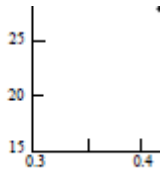

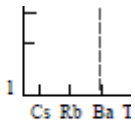

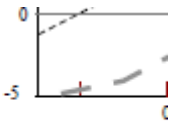

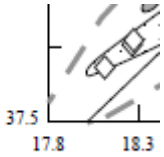

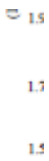

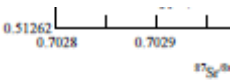

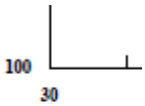

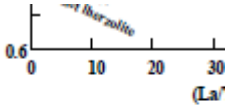

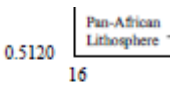

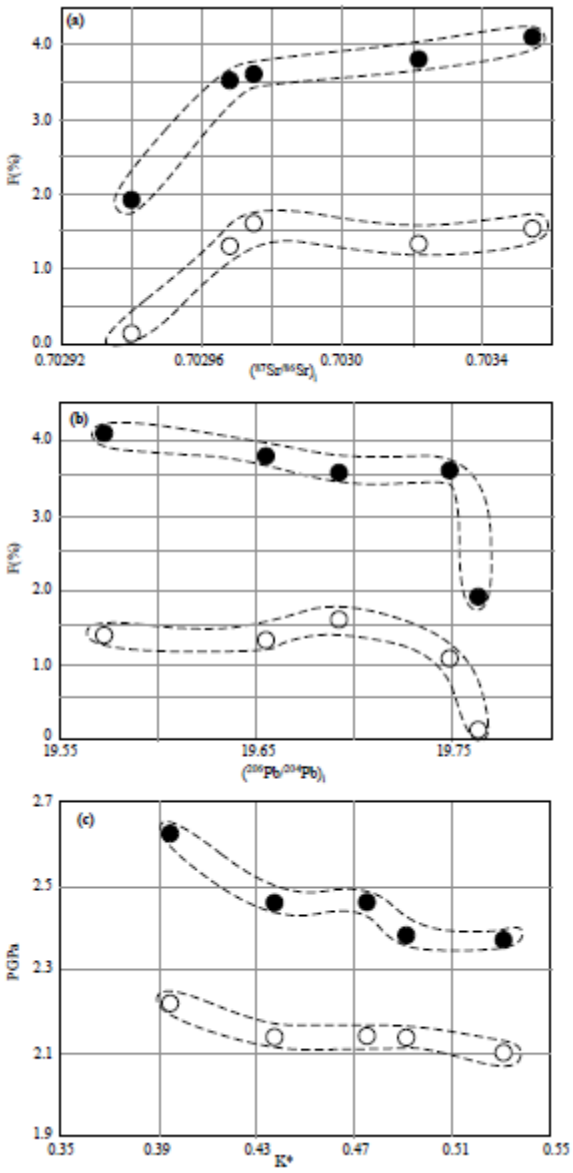

Fig.(11)

Table (1) Bulk composition and CIPW norm (wt%), of the basaltic lavas (OAB: olivine alkali basalt, BS: basanite and TB: trachybasalt) in the Natash volcanic province

Sample no.	NAT-3	NAT-5	NAT-7	NAT-8	NAT-9	NAT-11	NAT-12	NAT-13	NAT-14	M2001	M2001
Rock type	OAB	OAB	OAB	OAB	OAB	OAB	TB	BS	BS	OAB	TB
Major oxides (wt%)											
SiO_2	45.6	47.4	45.7	46.3	45.8	45.8	47.4	44.0	46.4	45.55	46.37
TiO_2	2.75	3.10	3.02	2.63	3.14	3.13	3.01	2.50	2.40	3.22	3.04
Al_2O_3	14.3	16.1	15.7	13.8	15.9	15.9	17.0	13.3	15.9	13.95	14.46
Fe_2O_3(Total)	13.3	13.5	13.0	12.2	13.3	13.3	12.9	13.1	15.0	14.17	13.92
MnO	0.19	0.19	0.18	0.17	0.18	0.18	0.20	0.20	0.25	0.18	0.18
MgO	8.91	5.55	6.75	9.10	6.12	6.33	4.22	10.56	3.72	7.55	6.29
CaO	8.98	7.85	8.39	9.80	8.50	8.38	6.84	10.61	5.99	8.71	7.90
Na_2O	3.38	3.51	3.25	2.61	3.44	3.18	4.55	2.59	4.91	3.24	3.9
K_2O	1.05	1.27	1.06	1.00	1.09	1.06	1.40	1.19	1.38	1.22	1.42
P_2O_5	0.56	0.94	0.70	0.48	0.70	0.70	0.82	0.57	1.90	0.64	0.74
LOI	1.25	1.87	1.77	1.16	1.57	2.08	1.53	1.02	2.23	1.22	1.25
Total	100.27	101.28	99.52	99.25	99.74	100.04	99.87	99.64	100.08	99.65	99.47
Mg#	0.570	0.449	0.507	0.596	0.476	0.486	0.393	0.615	0.329	50.99	46.48
CIPW (norm)											
Or	6.21	7.51	6.26	5.91	6.44	6.26	8.27	7.03	8.16	7.21	8.39
Ab	19.85	29.70	26.20	21.75	25.96	26.91	32.50	10.03	36.63	22.35	25.59
An	20.75	24.42	25.12	22.99	24.72	25.98	21.83	21.15	17.27	19.92	17.76
Ne	4.74		0.70	0.18	1.71		3.25	6.44	2.66	2.74	4.01
Di	16.53	6.98	9.86	18.39	10.68	9.14	5.67	22.67	0.04	15.79	13.79
Hy		3.76				0.31					
Ol	22.51	17.03	20.37	21.02	19.16	19.88	17.34	23.36	21.96	20.79	19.18
Mt	1.93	1.96	1.88	1.77	1.93	1.93	1.87	1.90	2.17	2.05	2.02
Il	5.22	5.89	5.74	5.00	5.96	5.95	5.72	4.75	4.56	6.12	5.77

Ap	1.30	2.18	1.62	1.11	1.62	1.62	1.90	1.32	4.40	1.48	1.72
Trace elements (ppm)											
Li	8.06	15.6	17.0	13.07	16.8	18.4	9.9	12.7	11.2		
Be	1.61	1.82	1.47	1.24	1.45	1.63	1.96	1.68	1.68		
Sc	23.6	19.4	22.1	25.7	22.5	24.5	14.5	27.4	8.5		
V	210	192	211	219	221	247	140	224	32.3		
Cr	370	41.0	137	412	96.6	95.8	3.31	378	1.73	207.6	140.4
Co	53.9	39.3	45.9	49.3	45.9	49.5	26.9	59.6	20.8		
Ni	205	24.6	75.8	150	44.7	47.9	0.90	225	0.85	156.6	133
Cu	50.6	18.5	28.1	41.6	22.8	25.0	6.38	63.2	6.96		
Zn	104	127	114	92.2	116.6	132	112	102	94.0		
Ga	19.1	22.1	21.0	17.5	21.3	23.1	20.1	18.9	15.5		
Rb	22.1	22.8	18.5	15.6	18.9	19.9	23.4	32.6	20.3	16.2	21.6
Sr	738	739	684	587	698	735	734	666	992	773	791
Y	28.5	34.9	29.9	24.6	30.2	33.6	37.6	28.8	38.4	27	34
Zr	251	323	263	226	263	293	351	271	292	235	303
Nb	67.4	78.8	59.9	53.4	61.1	61.1	81.9	81.1	73.9	51.3	66.2
Cs	0.34	0.31	0.25	0.15	0.75	0.30	1.71	0.35	0.53		
Ba	382	343	363	248	313	500	373	456	605	591	659
La	39	44	35.9	29.7	35.1	38.9	47.6	49.1	55.6	36.7	46.9
Ce	80.6	95.5	78.1	63.6	75.8	84.6	102	96.5	120	75.4	98.1
Pr	9.6	11.8	9.72	7.83	9.43	10.5	12.5	11.1	15.0	9.32	12.3
Nd	38.4	48.6	39.9	32.0	38.9	43.4	49.9	42.2	62.1	37.7	49.5
Sm	7.76	9.80	8.22	6.62	8.11	8.97	9.98	8.07	11.89	7.82	10.0
Eu	2.59	3.21	2.75	2.18	2.71	2.98	3.12	2.53	3.99	2.54	3.07
Gd	7.12	9.00	7.52	6.19	7.56	8.37	9.00	7.33	10.45	7.49	9.48
Tb	1.00	1.25	1.05	0.88	1.06	1.17	1.28	1.02	1.38	1.03	1.29
Dy	5.50	6.70	5.69	4.75	5.70	6.33	6.95	5.58	7.26	5.54	6.86
Ho	1.01	1.22	1.05	0.88	1.07	1.17	1.29	1.02	1.32	0.99	1.22
Er	2.57	3.05	2.62	2.18	2.67	2.93	3.32	2.61	3.25	2.66	3.25
Yb	2.04	2.38	2.04	1.74	2.10	2.31	2.68	2.09	2.46	2.14	2.66
Lu	0.28	0.32	0.28	0.24	0.29	0.32	0.38	0.29	0.34	0.33	0.4
Hf	5.22	6.53	5.34	4.74	5.40	5.92	6.89	5.67	5.69	5.75	7.29
Ta	4.12	4.98	3.84	3.29	3.89	3.94	5.25	5.15	3.58	3.38	4.08

W	1.03	0.02	0.61	0.77	1.05	1.02	1.67	1.98	1.05		
Pb	2.16	2.15	1.86	1.48	1.82	2.06	3.20	3.98	2.22		
Th	4.43	4.30	3.48	3.04	3.46	3.84	4.86	6.28	4.98	3.80	4.67
U	1.20	1.27	1.06	0.88	1.00	1.09	1.39	1.61	1.35	1.12	1.37

M2001 are average composition of olivine alkali basalts and trachybasats (hawaiites) from Natash volcanic province after Mohamed (2001).

Table (2) Sr-Nd-Hf-Pb isotope data for basaltic lavas from the Natash volcanic province

Sample	$^{87}Sr/^{86}Sr$ (2σ)	$(^{87}Sr/^{86}Sr)_i$	$^{143}Nd/^{144}Nd$ (2σ)	$(^{143}Nd/^{144}Nd)_i$	εNd_i	$^{176}Hf/^{177}Hf$ (2σ)	$(^{176}Hf/^{177}Hf)_i$	εHf
NAT-3	0.703049 (10)	0.702939	0.512783 (15)	0.512707	1.35	0.282811 (11)	0.282798	0.91
NAT -5	0.703087 (9)	0.702973	0.512798 (7)	0.512721	1.62	0.282805 (10)	0.282793	0.74
NAT -7	0.703068 (7)	0.702968	0.512807 (7)	0.512729	1.78	0.282809 (10)	0.282796	0.85
NAT -8	0.703073 (9)	0.702975	0.512793 (9)	0.512715	1.51	0.282795 (10)	0.282782	0.36
NAT -9	0.703122 (9)	0.703022	0.512806 (7)	0.512727	1.74	0.282811 (10)	0.282798	0.92
NAT-11	0.703127 (8)	0.703027	0.512805 (6)	0.512727	1.74	0.282800 (10)	0.282787	0.52
NAT-12	0.703157 (7)	0.703039	0.512793 (6)	0.512717	1.55	0.282810 (9)	0.282796	0.85
NAT-13	0.703195 (10)	0.703054	0.512725(7)	0.512653	0.29	0.282755 (10)	0.282742	0.01
NAT-14	0.702933 (8)	0.702858	0.512834(6)	0.512761	2.40	0.282865 (9)	0.282849	2.73

Table (2) *continue:*

Sample	$^{206}Pb/^{204}Pb$ (2σ)	$(^{206}Pb/^{204}Pb)_i$	$^{207}Pb/^{204}Pb$ (2σ)	$(^{207}Pb/^{204}Pb)_i$	$^{208}Pb/^{204}Pb$ (2σ)	$(^{208}Pb/^{204}Pb)_i$	Δ7/4	Δ8/4
NAT -3	20.311 (1)	19.763	15.764 (1)	15.737	40.142 (2)	39.474	10.54	-2.23
NAT -5	20.225 (1)	19.622	15.736 (1)	15.707	40.001 (1)	39.350	8.93	-0.02
NAT -7	20.330 (1)	19.748	15.742 (1)	15.714	40.049(3)	39.439	8.28	-6.31
NAT -8	20.300 (1)	19.691	15.744 (1)	15.715	40.073 (2)	39.404	8.90	-2.95
NAT -9	20.215 (1)	19.655	15.732 (1)	15.705	39.970 (3)	39.352	8.38	-3.84
NAT-11	20.205 (1)	19.664	15.731 (1)	15.705	39.952 (2)	39.343	8.27	-5.73
NAT-12	19.723 (1)	19.279	15.699(1)	15.678	39.541 (3)	39.046	9.73	10.99
NAT-13	19.986 (1)	19.573	15.760 (1)	15.740	39.940 (2)	39.335	12.73	14.46
NAT-14	20.565 (1)	19.944	15.728 (1)	15.699	40.160 (2)	39.428	4.58	-31.15

Initial ratios are calculated at 90 Ma using the natural abundances of the parent-daughter isotopes. εNd and εHf are calculated with $^{143}Nd/^{144}Nd=0.512638$ and $^{176}Hf/^{177}Hf=0.282772$ (Blichert-Toft and Albarède, 1997); $\Delta 7/4= [(^{207}Pb/^{204}Pbs)_{initial} - (0.1084 \times (^{206}Pb/^{204}Pbs)_{initial} + 13.491)] \times 100$; $\Delta 8/4= [(^{208}Pb/^{204}Pb)_{initial} - (1.209 \times (^{206}Pb/^{204}Pb)_{measured} +15.627)] \times 100$.

Table (3) Starting compositions of NAT-14, NAT-13 basaltic samples and crust contaminant used to calculate the bulk and AFC trajectories in Figure 7

	Sr (ppm)	Nd (ppm)	$(^{87}Sr/^{86}Sr)_i$	$(^{143}Nd/^{144}Nd)_i$
Starting compositions				
Least contaminated starting composition based on isotope ratios (sample NAT-14)				
(a) Fractionation-corrected melt calculated under oxidizing conditions (F_2O_3/TiO_2 ~ 1)				
	494.3	32.5	0.7028589	0.512761
(b) Fractionation-corrected melt calculated under reducing conditions (Fe_2O_3/TiO_2 ~ 0.5)				
	459.5	30.2	0.702858	0.512761
Least fractionated starting composition based on bulk chemistry (sample NAT-13)				
(a) Fractionation-corrected melt calculated under oxidizing conditions (Fe_2O_3/TiO_2 ~ 1)				
	589.1	37.7	0.703054	0.512653
(b) Fractionation-corrected melt calculated under reducing conditions (Fe_2O_3/TiO_2 ~ 0.5)				
	506.1	32.2	0.703054	0.512653
Starting composition of granulite-facies late-Proterozoic lower crust				
	538	9.45	0.703363	0.512620

Table (4) Intensive and extensive melting parameters for Natash mafic volcanics

Samples	Tp (^{o}C) [1]	P_M GPa[1]	P_M GPa [2]	$T^{Ol\text{-}L}$ (^{o}C) [1]	Ts (^{o}C) [2]	F(%)[1]	(Fo^{Ol})[1]	KD^{O-L}_{Fe-Mg}
NAT-03	(1366-1420)	(1.6-1.9)	(2.0-2.4)	(1394- 1436)	(1406-1450)	(0.1-1.9)	(88.32-88.70)	(0.342-0.344)
NAT-07	(1360-1424)	(1.4-1.7)	(2.0-2.4)	(1379- 1427)	(1405-1455)	(1.1-3.6)	(88.70-88.94)	(0.343-0.344)
NAT-08	(1395-1400)	(1.7-1.7)	(2.1-2.3)	(1411-1412)	(1440-1440)	(1.6-3.6)	(88.94-89.96)	(0.343-0.343)
NAT-09	(1347-1415)	(1.3-1.6)	(2.0-2.3)	(1360-1414)	(1394-1448)	(1.3-3.8)	(88.75-89.29)	(0.342-0.343)
NAT-13	(1385-1441)	(1.9-2.3)	(2.1-2.6)	(1414-1436)	(1420-1453)	(1.4-4.1)	(88.71-89.09)	(0.339-0.342)

All fractionation-corrected melts used in calculations show primary melt criteria (e.g. 68-72 Mg#, 300-500 ppm Ni, >33 ppm Sc) and involve ~~an~~ olivine in the mineral assemblage that add to the liquid line of descent (LLD). Brackets display parameters of the corrected melts under oxidizing (first figures) and reducing (second figures) conditions (see text for details). Potential temperatures (T_P) [1], melting pressure (P_M)[1] , olivine-melt equilibrium temperature $T^{Ol\text{-}L}$ (^{o}C) [1], melt fraction F(%)[1], predicted Fo compositions and KD^{O-L}_{Fe-Mg} are calculated from (Putirka, 2016), whereas melting pressure (P_M)[2] and solidus temperature (Ts) [2] are calculated from Herzberg and Asimow (2015).

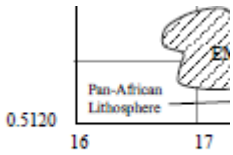

Graphical abstract

Multicomponents melting source of the Natash volcanics in the terms of Sr-Nd-Pb-isotopic ratios

Highlights

-The Natash lavas show correlations between isotopic ratios and major and trace elements

- Crustal assimilation cannot explain these correlations and melting in a multicomponent source is invoked

- HIMU, EM-I and DM domains are present in the mantle source within the lithosphere

- Source heterogeneity resulted from hydrous fluid flux during Pan-African Orogeny.

- Upwelling asthenosphere induced lithosphere melting in Late Cretaceous.